Nanoscale

ROYAL SOCIETY OF CHEMISTRY

REVIEW

View Article Online
View Journal | View Issue

Check for updates

Cite this: *Nanoscale*, 2024, **16**, 8256

High-entropy-based nano-materials for sustainable environmental applications

Shubhasikha Das,[a] Shamik Chowdhury*[a] and Chandra Sekhar Tiwary *[b]

High entropy materials (HEMs), epitomized by high entropy alloys (HEAs), have sparked immense interest for a range of clean energy and environmental applications due to their remarkable structural versatility and adjustable characteristics. In the face of environmental challenges, HEMs have emerged as valuable tools for addressing issues ranging from wastewater remediation to energy conversion and storage. This review provides a comprehensive exploration of HEMs, spotlighting their catalytic capabilities in diverse redox reactions, such as carbon dioxide reduction to value-added products, degradation of organic pollutants, oxygen reduction, hydrogen evolution, and ammonia decomposition using electrocatalytic and photocatalytic pathways. Additionally, the review highlights HEMs as novel electrode nanomaterials, with the potential to enhance the performance of batteries and supercapacitors. Their unique features, including high capacitance, electrical conductivity, and thermal stability, make them valuable components for meeting crucial energy demands. Furthermore, the review examines challenges and opportunities in advancing HEMs, emphasizing the importance of understanding the underlying mechanisms governing their catalytic and electrochemical behaviors. Essential considerations for optimizing the HEM performance in catalysis and energy storage are outlined to guide future research. Moreover, to provide a comprehensive understanding of the current research landscape, a meticulous bibliometric analysis is presented, offering insights into the trends, focal points, and emerging directions within the realm of HEMs, particularly in addressing environmental concerns.

Received 1st February 2024,
Accepted 20th March 2024

DOI: 10.1039/d4nr00474d

rsc.li/nanoscale

Published on 20 bezna 2024. Downloaded on 01.02.2026 4:42:30.

1. Introduction

In 2004, a significant advancement was made in the design and construction of alloys, which involved incorporating numerous principal elements. This group of alloys was subsequently named 'high entropy alloys' (HEAs).[1,2] This discovery has significantly propelled advancements in the field of materials science and engineering and fundamentally altered the way we understand alloys. HEAs are characterized as alloys composed of a minimum of five principal elements, each with concentrations ranging from 5 to 35 at.%.[3] HEAs are anticipated to demonstrate exceptional properties, attributed to their distinctive metallurgical characteristics resulting from the presence of multiple alloying elements. This unique composition makes them well suited for various engineering applications (Fig. 1).[4–6] Moreover, the advanced properties and distinct advantages of HEAs have inspired researchers to investigate alternative high entropy materials (HEMs), derived from the principles of HEAs. As a result, the burgeoning field of HEMs, encompassing alloys and ceramics, such as high entropy nitrides,[7] carbides,[8] and oxides,[9] has witnessed rapid growth in materials research.

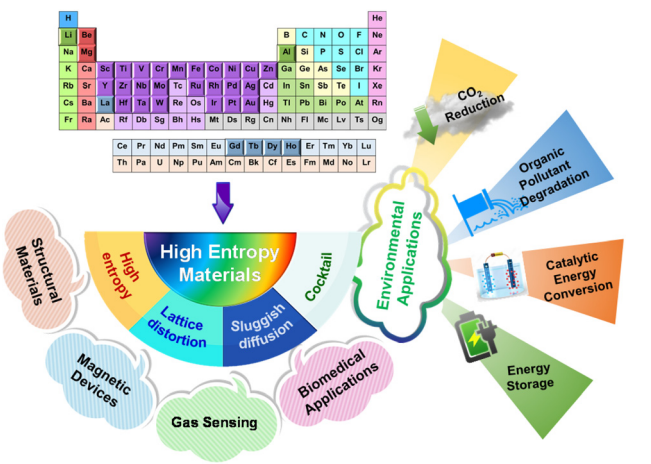

Fig. 1 The diverse applications of HEMs, highlighting their unique properties, with a particular focus on their environmental applications.

[a]*School of Environmental Science and Engineering, Indian Institute of Technology Kharagpur, West Bengal 721302, India. E-mail: shamikc@iitkgp.ac.in*
[b]*Department of Metallurgical and Materials Engineering, Indian Institute of Technology Kharagpur, West Bengal 721302, India. E-mail: chandra.tiwary@metal.iitkgp.ac.in*

This journal is © The Royal Society of Chemistry 2024

Published on 20 bezna 2024. Downloaded on 01.02.2026 4:42:30.

Numerous studies have unveiled a diverse array of structural characteristics within this expansive range of materials, spanning from cryogenic ductility, robust strength, and corrosion resistance to exceptional wear resistance and thermoelectric properties.[10–12] Therefore, HEMs are experiencing increasing adoption in industrial, aerospace, and welding applications, as well as in the construction of heat exchangers and high-temperature furnaces.[13,14] Furthermore, within the realm of magnetism, HEMs containing magnetic ions have emerged as a versatile platform for tuning magnetic properties. Recent studies have demonstrated that the intricate interplay between local cationic disorder and the concentration of magnetic ions contributes to enhanced exchange coupling, making these materials conducive for applications in magnetic memory devices, magnetometers, and magneto-optical devices.[15,16] Apart from magnetism applications, HEMs have found remarkable utility in gas-sensing applications.[17] Their complex microstructures, characterized by a high density of grain boundaries and interfaces, facilitate efficient gas–surface interactions. This property translates into heightened sensitivity towards gases such as hydrogen,[18,19] methane,[20] carbon dioxide (CO_2),[21] and triethylamine.[22] Intriguingly, HEMs have also made notable strides in biomedical applications, particularly as metallic implant materials.[11] These materials overcome challenges, including stress shielding, substantial fatigue resistance, high yield strength, and exceptional ductility by offering elastically isotropic systems with low Young's moduli.[23,24]

In the prevailing circumstances, HEMs are receiving increased attention that extends beyond their conventional roles in structural and functional applications. This heightened focus is specifically directed toward leveraging HEMs to effectively address a diverse range of environmental concerns. From wastewater remediation to energy conversion and storage, and even in the critical realm of CO_2 reduction, HEMs are emerging as valuable tools to combat pressing environmental issues. In the face of ongoing environmental concerns, such as the impending threat of climate change and increasing CO_2 levels in the atmosphere, HEMs offer potential breakthroughs in converting CO_2 to value-added products,[25] presenting a novel avenue for mitigating greenhouse gas emissions and combating climate change. Nonetheless, HEMs exhibit excellent potential in the realm of wastewater remediation by effectively degrading various emerging contaminants.[26] This contributes significantly to the improvement of water systems, ensuring cleaner water resources. Moreover, in the context of energy conversion and storage, HEMs offer innovative solutions to promote more efficient and sustainable energy practices through water splitting[27] and ammonia decomposition,[28] addressing the urgent need for cleaner and renewable energy sources. The exceptional physicochemical and surface characteristics of these materials, marked by their outstanding catalytic activity and remarkable stability, surpass those exhibited by binary and ternary alloys, making them outstanding materials for efficiently addressing environmental concerns.[19,29,30] These applications leverage the distinctive structural and electronic features inherent in HEMs, showcasing their adaptability and effectiveness across a broad spectrum of pivotal processes. By diversifying their applications across these environmental fronts, HEMs have emerged as versatile tools in the quest for eradicating contemporary environmental challenges and fostering a more sustainable and ecologically balanced future.

In view of the aforementioned, this review encapsulates fundamental concepts and the current depth of knowledge concerning HEMs. It delves into the intrinsic effects and distinctive properties of HEMs. Additionally, to assess the current research landscape of HEMs, a bibliometric analysis is conducted. This analysis serves as a navigational tool, offering a panoramic view of the present state of HEM research. Furthermore, it helps in identifying trends, influential studies, and potential directions for future research. The review further emphasizes the evolving landscape of environmental applications, shedding light on the promising role that HEMs can play in mitigating various environmental concerns. In addition, this review also sheds light on different challenges associated with the applications of HEMs and attempts to identify critical issues to be considered while designing HEMs with improved performances. Therefore, the current review is anticipated to be beneficial for researchers, environmental engineers, and scientists involved in materials research and applications.

2. Methodology

The online database Scopus was accessed on 25th November 2023. The data were extracted from the platform to conduct a comprehensive bibliometric analysis of the publication landscape concerning HEMs. The related articles were identified through a search employing keywords such as "high entropy" AND "catalysis" OR "water splitting" OR "oxygen evolution" OR "hydrogen evolution" OR "CO_2 reduction" OR "ammonia decomposition" OR "organic pollutant degradation" OR "battery" OR "supercapacitor". All document types were included for bibliometric analysis. The relevant articles resulting from the search were then exported in the CSV format in order to extract the abstract, keywords, and citation details. Subsequently, the Scopus database was imported into the VOSviewer software (version 1.6.17, Leiden University, Netherlands) for bibliometric mapping.[31]

3. Bibliometric analysis of HEMs

A network visualization map of keywords related to "high entropy" is depicted in Fig. 2a. The keyword "entropy" is emphasized due to its frequent occurrence and extensive connections. Using VOSviewer software, the keywords were grouped into 5 clusters: red, blue, green, yellow, and purple, depicting the interrelationships between the different topics. The red cluster focuses on various applications of high entropy

Published on 20 bezna 2024. Downloaded on 01.02.2026 4:42:30.

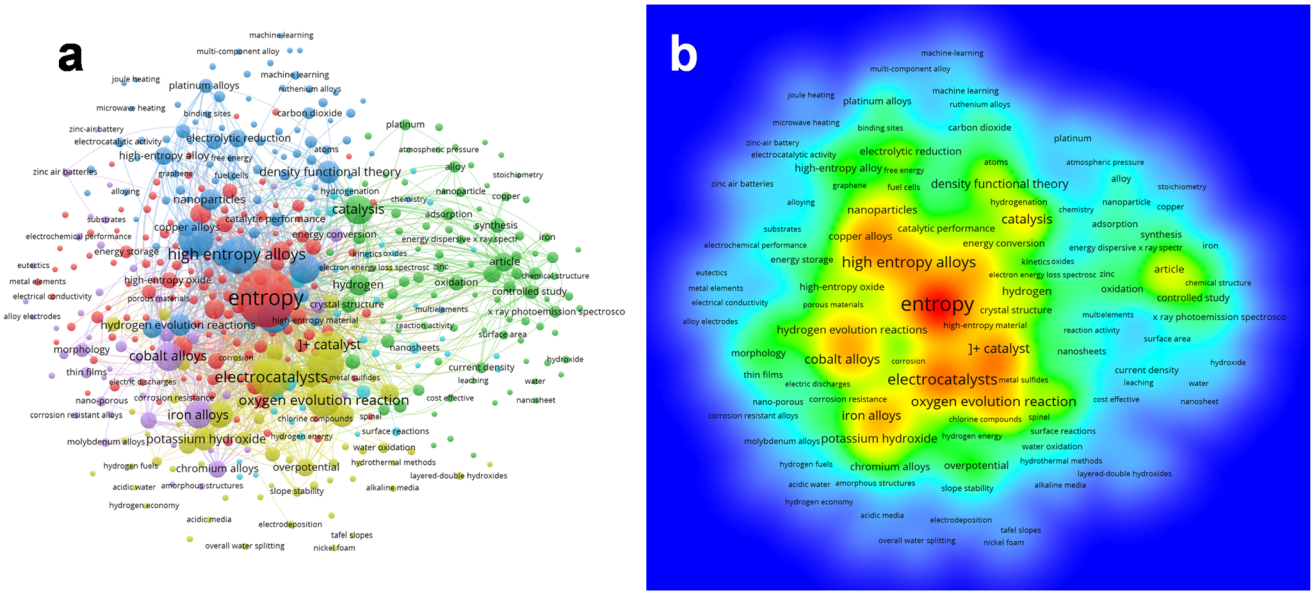

Fig. 2 (a) Network view map and (b) density visualization map of keyword occurrences as generated from VOSViewer.

materials, spanning across energy and catalytic conversions, fuel cells, and corrosion resistance, among others. Meanwhile, the blue cluster revolves around alloy design, and encompasses high entropy alloys, density functional theory (DFT), nanoparticles (NPs), and catalytic performance. Keywords linked to material characteristics, such as synthesis, adsorption, specific surface area, current density, and reactivity, are clustered under green. The yellow cluster comprises keywords related to electrocatalysis, such as catalyst, the oxygen evolution reaction, overpotential, potassium hydroxide, and slope stability. Lastly, the purple cluster includes keywords like cobalt alloys, iron alloys, and chromium alloys, highlighting the diverse composition of HEMs. Additionally, Fig. 2b delineates the density visualization of the keywords associated with "high entropy". The visualization is presented using a rainbow color scheme, where red denotes high density and blue signifies low density. Notably, entropy emerges as the major hotspot, as indicated by the red color (Fig. 2b). The yellow color observed in the surrounding points signifies a strong correlation with the focal areas. In Fig. 2b, it is evident that catalysis, electrocatalysts, the oxygen evolution reaction (OER), the hydrogen evolution reaction (HER), *etc.*, are closely associated with the hotspots (entropy and high entropy alloys) because of the various application domains.

4. Environmental applications of HEMs

4.1. Carbon dioxide reduction reaction

With the notable surge in anthropogenic CO_2 emissions from intensified fossil fuel burning activities, there is a pressing need to reduce the influx of this greenhouse gas into the atmosphere.[32] Electrocatalytic and photocatalytic CO_2 reduction pathways present viable solutions for establishing a closed-loop carbon cycle (Fig. 3a). These approaches offer potential avenues to tackle the issue of excessive CO_2 emissions by transforming CO_2 into valuable compounds like methane, ethylene, and ethanol.[33,34] Accordingly, a variety of catalysts, including metal oxides, metal sulfides, and carbon-based materials, have been exploited to produce various chemical fuels by the electrocatalytic CO_2 reduction reaction (CO_2RR). However, poor selectivity and low faradaic efficiency stand out as key issues. These hurdles stem from catalysts with inadequate activity in C–C coupling reactions, limiting the generation of carbonaceous products. Therefore, it is crucial to develop highly efficient and selective electrocatalysts that support the CO_2RR. Recently, HEAs have gained attention as a potential class of catalysts for CO_2RR. In a notable study, a AuAgPtPdCu HEA was used as an electrocatalyst for CO_2RR.[25] When compared to the catalysis in N_2 saturated solution, the cathodic current density in the CO_2 saturated electrolyte reached 10.15 mA cm^{-2} at a potential of 0.8 V *versus* Ag/AgCl, suggesting its superior catalytic activity. (Fig. 3b–d). Similar to other Cu-based electrocatalysts, the quinary AuAgPtPdCu HEA could produce a variety of gaseous products, such as CO, CH_4, C_2H_4, and H_2 in the CO_2RR process. At a low applied voltage of −0.3 V, the HEA catalyst achieved a faradaic efficiency of around 100% toward gaseous products. Although the majority of the electrocatalytic activity of the HEA catalyst was due to Cu atoms, other metals also played synergistic roles in the CO_2RR process.

Meanwhile, extensive research is also underway to investigate diverse HEMs to improve the efficiency of the CO_2RR through enhanced photocatalytic performance. For example, a defective high entropy oxide (HEO) $TiZrNbHfTaO_{11}$ was synthesized and employed for photocatalytic CO_2 conversion.[35]

 This journal is © The Royal Society of Chemistry 2024

Published on 20 bezna 2024. Downloaded on 01.02.2026 4:42:30.

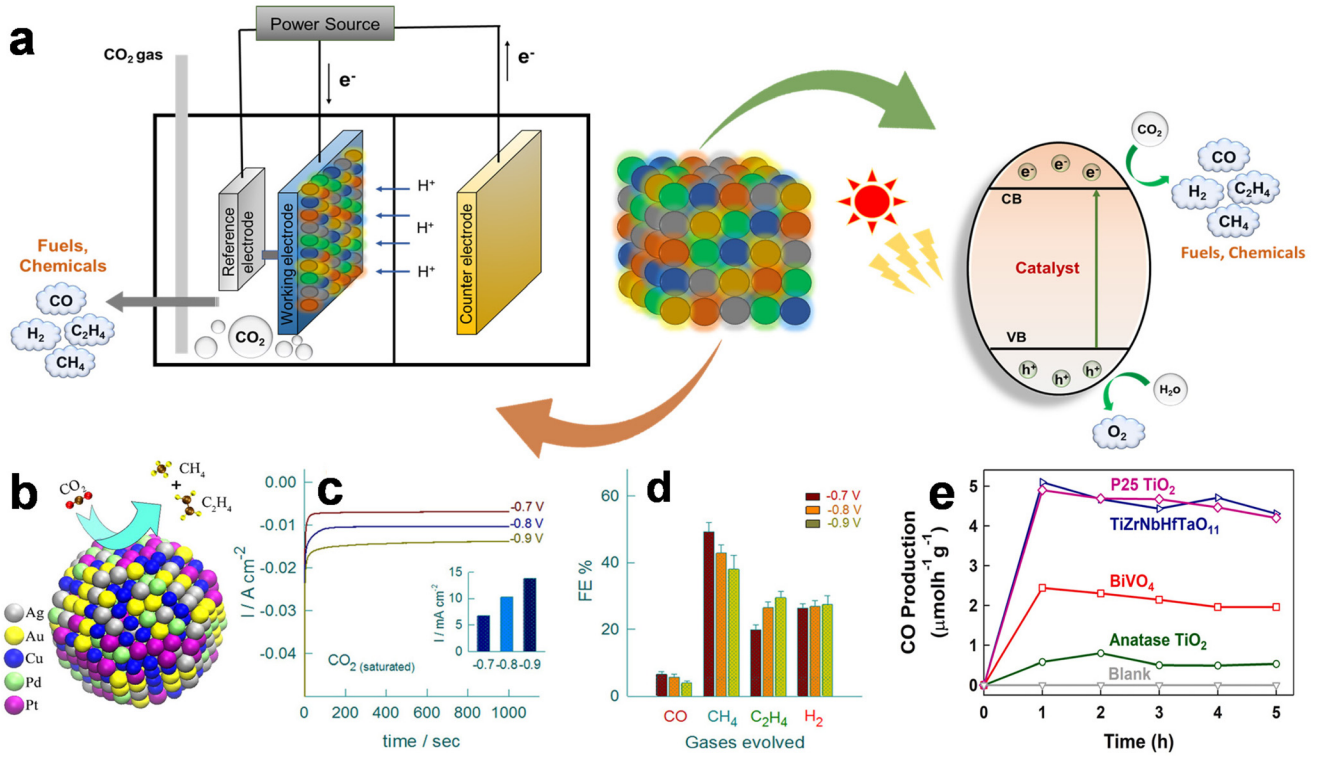

Fig. 3 (a) Schematic of CO_2 reduction by electrocatalysis and photocatalysis using HEMs. (b) Illustration of the catalytic reduction of CO_2 by AuAgPtPdCu nanoparticles. (c) Comparison of the chronoamperometric responses in CO_2-saturated electrolyte at different potentials for 1000 s, and (d) bar diagram for the faradaic efficiencies of their respective carbonaceous species and hydrogen gaseous products. Reproduced from ref. 25 with permission from the American Chemical Society, Copyright 2020. (e) Comparison of the efficiency of $TiZrNbHfTaO_{11}$ with TiO_2 and $BiVO_4$ for photocatalytic CO_2 conversion. Reproduced from ref. 35 with permission from Elsevier, Copyright 2022.

Compared to some of the most widely used photocatalysts for CO_2 conversion, such as anatase TiO_2 and $BiVO_4$, the HEO produced substantially more CO (Fig. 3c). Oxygen vacancies within the lattice, active sites accommodating five cations, an appropriate electronic structure facilitating CO_2 conversion, and prolonged lifespan of charge carriers participating in photocatalysis were highlighted as the key factors driving the increased CO production by the HEO. Indeed, these findings on HEA-based materials demonstrate their potential for successful CO_2 conversion using various catalytic processes.

4.2. Degradation of organic pollutants

The escalating discharge of organic contaminants into water bodies, propelled by global population growth and industrialization, poses a substantial environmental challenge.[36,37] Traditional wastewater treatment methods struggle to mineralize these complex compounds, necessitating innovative approaches.[38] Heterogeneous photocatalysis, a facet of advanced oxidation processes (AOPs), has emerged as a practical and efficient means of treating wastewater. This technique harnesses highly active oxygen-based radicals to break down organic pollutants into harmless compounds. Yet, it faces significant limitations with regard to conventional transition-metal-based catalysts due to availability, cost, and toxicity. In this context, HEMs have captured enormous attention for their potential to catalyse the photodegradation of organic pollutants. For instance, the $(Ni_{40}Fe_{30}Co_{20}Al_{10})_{90}Ti_{10}$ as-milled HEA exhibited exceptional performance in degrading methyl blue under visible light, attributed to lattice distortion, multielement active sites, efficient charge transfer, narrow bandgap, and photon absorption of longer wavelengths.[39] In another investigation, the FeCoNiCuZn HEA with n-type semiconductor properties has demonstrated remarkable photocatalytic activity for eliminating various pharmaceutical residues (tetracycline ~86%, sulfamethoxazole ~94%, ibuprofen ~80%, and diclofenac ~99%) from water bodies under visible light.[26] Similarly, the MnFeCoNiCu HEA has been found to demonstrate superior activity over conventional photocatalysts in degrading antibiotics (sulfamethoxazole ~95%, ofloxacin ~94%, and ciprofloxacin ~89%) under visible light,[40] especially in real water matrixes (Fig. 4a). It was reported that visible light photocatalysis on HEA NPs is primarily initiated through the reduction of oxygen molecules adsorbed onto active sites by photogenerated electrons. This reduction process leads to the generation of superoxide anions ($^{\bullet}O_2^-$) and facilitates multi-redox reactions, yielding hydroxyl radicals ($^{\bullet}OH$). Both $^{\bullet}O_2^-$ and $^{\bullet}OH$ radicals, in conjunction with photoinduced valence band holes, orchestrate the oxidation of the reactant mole-

Published on 20 bezna 2024. Downloaded on 01.02.2026 4:42:30.

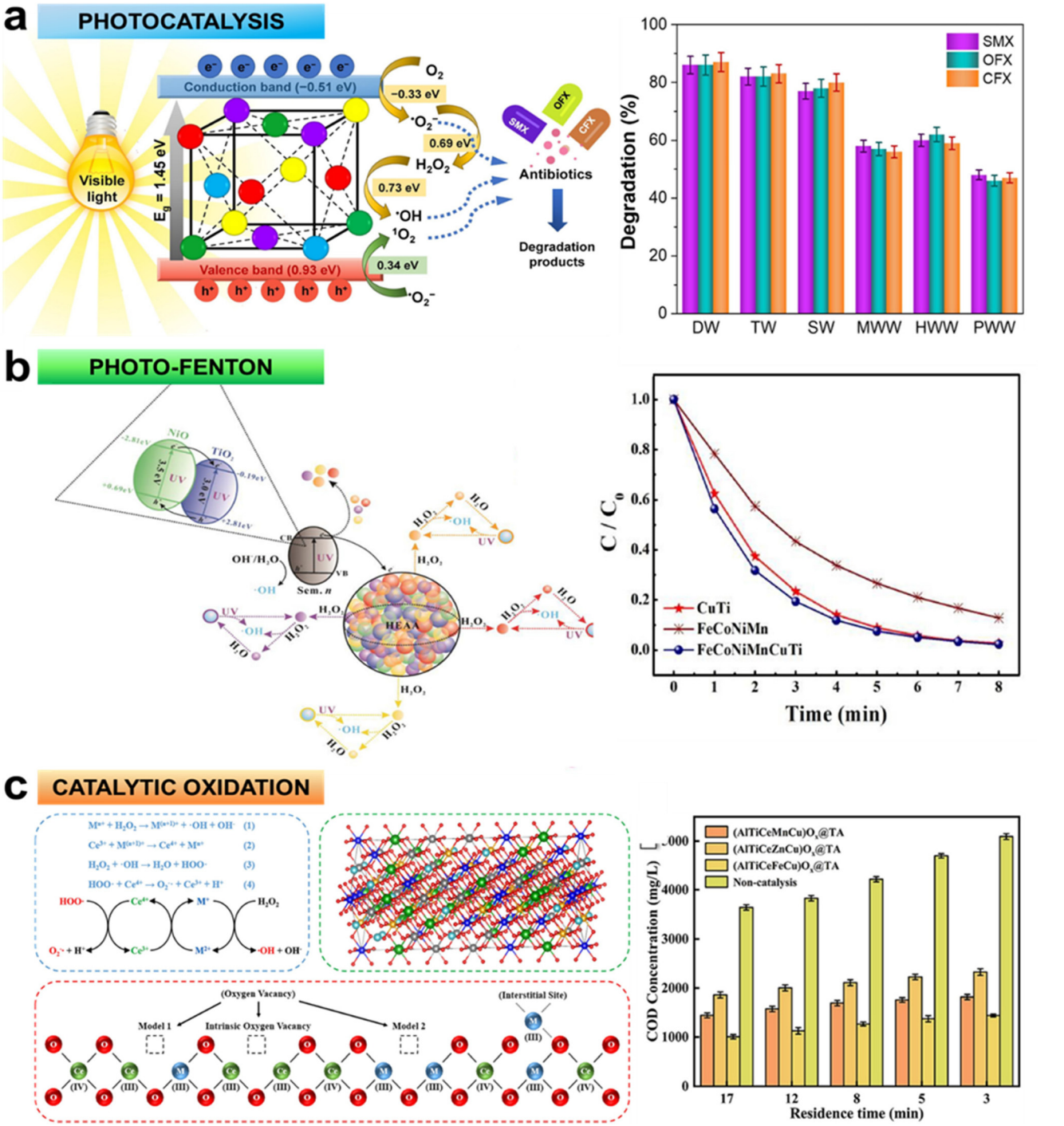

Fig. 4 Degradation mechanisms and efficacy of three distinct AOPs: (a) MnFeCoNiCu NPs for the photocatalytic degradation of a ternary mixture of sulfamethoxazole (SMX), ofloxacin (OFX), and ciprofloxacin (CFX) in different water matrixes (DW: deionized water, TW: tap water, SW: surface water, MWW: municipal wastewater, HWW: hospital wastewater, PWW: pharmaceutical industry wastewater), reproduced from ref. 40 with permission from Elsevier, Copyright 2023; (b) FeCoNiMnCuTi-based photo-Fenton system for decomposition of rhodamine B, reproduced from ref. 42 with permission from Elsevier, Copyright 2022; and (c) ultrafast catalytic oxidation system employing (AlTiCeMCu)O_x@TiO_2-Al_2O_3 catalyst for dissociation of methylene blue and rhodamine B, reproduced from ref. 43 with permission from Elsevier, Copyright 2022.

cules. Moreover, a fraction of $^{\bullet}O_2^-$radicals is likely oxidized by valence band holes to form singlet oxygen ($^1O_2$), thereby further contributing to the photocatalytic degradation of contaminants.[40]

In tandem with photocatalysis, HEAs have also been proposed for heterogeneous Fenton-like processes (Fe^{2+}/Fe^{3+}+H_2O_2) for dye degradation. The challenges of traditional Fenton methods, including a limited range of operating pH

 This journal is © The Royal Society of Chemistry 2024

Published on 20 bezna 2024. Downloaded on 01.02.2026 4:42:30.

and poor catalytic stability of zero-valent iron-based catalysts, motivate the exploration of HEAs in this domain.[41] HEAs like FeCoNiMnCuTi demonstrated enhanced photo-Fenton activity for rhodamine B decomposition.[42] This could be attributed to several key factors: (i) inclusion of potent Fenton-active elements (Fe and Cu) in the alloy; (ii) Co and Mn in the alloys extending the pH range for Fenton activity; (iii) Ni and Ti enhancing catalytic stability of the alloy; and (iv) the combined effects of heterogeneous photo-Fenton and semiconductor photocatalysis (Fig. 4b) during dye decomposition.

Additionally, HEAs are gaining attention in ultra-fast oxidation technology, thereby intensifying wet oxidation processes to efficiently treat heterocyclic compounds. For example, the $(AlTiCeMCu)O_x@TiO_2$-Al_2O_3 (M = Mn, Zn, Fe) catalyst exhibited remarkable efficiency in degrading synthetic pollutants like methylene blue and rhodamine B (Fig. 4c), leveraging the catalytic efficiency of each active component in a high entropy state.[43] These studies collectively illuminate the potential of HEAs in AOPs, offering effective and sustainable solutions for treating complex organic contaminants, often present in various water bodies.

Meanwhile, nitrate (NO_3^-) contamination in water bodies seems to present a significant threat to both ecosystems and human health by disrupting the global nitrogen cycle.[44,45] Its presence can lead to eutrophication, harmful algal blooms, and various health issues upon ingestion. In response, the electrocatalytic nitrate reduction reaction (NO_3RR) presents a viable solution to convert NO_3^- into ammonia (NH_3), thereby offering a means to rejuvenate the nitrogen cycle and remediate wastewater. This approach stands out as a green alternative to the energy-intensive Haber–Bosch process, which contributes significantly to global CO_2 emissions.[46,47] Furthermore, nitrate offers distinct advantages over dinitrogen due to its higher solubility and lower dissociation energy.[48,49] In recent years, significant progress has been made in the NO_3RR, leveraging various catalysts such as Cu encapsulated in porous carbon,[50] Fe-based single-atom catalysts,[51] MXene materials,[52] CuPd nanocubes,[53] and noble metal-based catalysts.[54] Despite these advancements, the rational design of catalysts with optimal activity, selectivity, and stability remains a key challenge.

Recent studies have highlighted the remarkable potential of HEMs as efficient catalysts for electrochemical nitrate reduction to NH_3. One study investigated the NO_3RR performance of FeCoNiCuZn through computational modeling such as first-principles DFT calculations and Monte Carlo simulations.[55] The study revealed that the (100) crystal plane of FeCoNiCuZn exhibited favorable adsorption energies for NO_3^-, resulting in ultra-low overpotentials and kinetic barriers. Further analysis identified the bridge site of Co–Co as the most effective reaction site for NO_3RR, with an exceptional selectivity of 99.9% towards NH_3 production and suppression of the HER. The superior electrocatalytic activity of the FeCoNiCuZn HEA was attributed to the positioning of the *d*-band center in its electronic structure. In another study, researchers explored the catalytic potential of a rock-salt HEO, $Mg_{0.2}Co_{0.2}Ni_{0.2}Cu_{0.2}Zn_{0.2}O$, for electrochemical NO_3RR.[56] This multi-component platform demonstrated impressive catalytic performance, achieving high faradaic efficiency (99.3%) and yield rates (26.6 mg mg_{cat}^{-1} h^{-1}) for NH_3 generation. The synergistic effect between Cu and Co was highlighted as a key factor contributing to the enhanced catalytic activity. Moreover, the modulation of intermediate adsorption energies and suppression of N–N formation through a multi-component platform further improved the catalytic efficiency of the HEO catalyst. Overall, these studies emphasise the advantages of HEMs over conventional catalysts for electrochemical NO_3RR. By leveraging the unique properties of HEMs, such as their diverse compositions and tailored electronic structures, researchers can design highly efficient and selective catalysts for NO_3RR.

4.3. Catalytic energy conversion

4.3.1. Oxygen evolution reaction. Water splitting holds significant importance in numerous technological realms, such as fuel cells, solar energy production, and catalysis. This technique efficiently generates molecular hydrogen at the cathode and oxygen at the anode utilizing readily available water.[57] The OER plays a critical role in the electrochemical water splitting process.[58] This step demands a considerable amount of energy and is crucial for the overall efficiency of the process.[59,60] Despite having outstanding OER activity, noble metal oxides (such as RuO_2 and IrO_2) have certain limitations that restrict their wide-scale applications, including exorbitant cost, noble nature, and poor long-term stability.[61–63] Therefore, a robust, effective, inexpensive, and stable non-noble metal-based OER catalyst is the need of the hour.

To this end, HEAs have emerged as a promising electrode material for OER under both acidic and alkaline conditions. (Fig. 5a). For instance, FeCoNiCrAl and FeNiMnCrCu HEAs were examined as catalysts for OER.[64] The results highlighted that the FeNiMnCrCu catalyst exhibited lower overpotential compared to the Pt catalyst with similar activity. The enhanced activity was attributed to significant lattice distortion. Moreover, substituting Co and Al with Mn and Cu boosted the catalytic activity due to a shift in lattice spacing. In another study, the AlNiCoIrMo catalyst was tested for water splitting in an alkaline environment,[65] resulting in a decreased onset potential of 1.42 V than IrO_2 (1.48 V), and a smaller Tafel slope of 55.2 mV dec^{-1} compared to other ternary and quaternary alloys reported in the literature (Fig. 5b). It was proposed that the alloying with several elements produces a high-entropy effect and a slow diffusion impact, which contribute to the increase in catalytic performance. Apart from HEAs, their oxides have also shown tremendous potential as electrocatalysts for OER. For instance, a $(CoNiMnZnFe)_3O_{3.2}$ HEO showcased a significantly lower overpotential of 336 mV at 10 mA cm^{-2} and a Tafel slope of 47.5 mV dec^{-1}.[66] These results surpassed the performance of individual metal oxide NPs, as illustrated in Fig. 5c and d. Other than HEOs, high entropy sulfides like $FeNiCoCrMnS_2$ have also demonstrated high reactivity at a current density of 10 mA cm^{-2} with overpotentials of

Published on 20 bezna 2024. Downloaded on 01.02.2026 4:42:30.

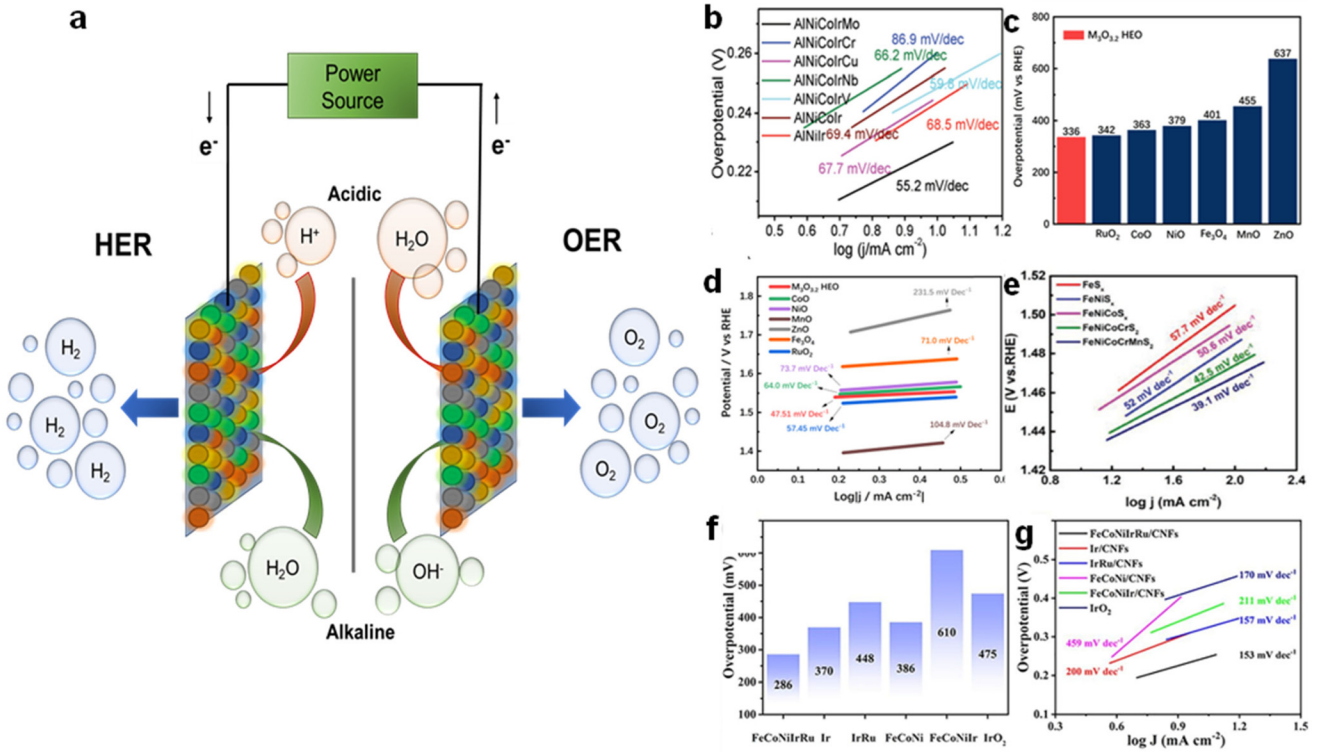

Fig. 5 (a) Schematic of water splitting reactions under acidic and alkaline conditions using HEMs as electrodes. (b) Tafel slopes of AlNiCoIrMo and IrO_2. Reproduced from ref. 65 with permission from John Wiley and Sons, Copyright 2019. (c) Overpotential values at a current density of 10 mA cm^{-2} and (d) Tafel slopes of $(CoNiMnZnFe)_3O_{3.2}$ HEO and its counterparts. Reproduced from ref. 66 with permission from Elsevier, Copyright 2021. (e) Tafel slopes of $FeNiCoCrMnS_2$. Reproduced from ref. 67 with permission from John Wiley and Sons, Copyright 2021. (f) Overpotential values at a current density of 20 mA cm^{-2} and (g) Tafel slopes of FeCoNiIrRu HEA supported on CNFs. Reproduced from ref. 68 with permission from Elsevier, Copyright 2022.

199 mV, exceeding unary metal as well as binary, ternary, and quaternary alloys (Fig. 5e).[67] It is speculated that the resultant metal (oxy)hydroxide from the self-reconstruction of the sulfides is the actual active component of the OER. Furthermore, FeCoNiIrRu HEA NPs supported on carbon nanofibers (CNFs) were also explored as OER catalysts.[68] These NPs display intriguing OER activity with a low overpotential of 241 mV at a current density of 10 mA cm^{-2} in acidic electrolytes (Fig. 5f and g). Furthermore, in a recent study, researchers delved into the realm of metal–organic frameworks (MOFs) to develop high-entropy MOF-based electrocatalysts for OER. By synthesizing individual metal-rich high entropy MOFs, Yao *et al.*[69] aimed to uncover a suitable unsaturated coordination environment for the metal active center. Their findings displayed the remarkable performance of a Co-rich high entropy MOF, showcasing its ability to significantly lower the overpotential to 310 mV at a current density of 10 mA cm^{-2}. Additionally, a number of HEMs, including high entropy phosphides,[70] borides,[71] fluorides,[72] *etc.*, have also shown promise as effective OER electrocatalysts as summarized in Table 1. The enhanced electrochemical stability of these materials stems from the collaborative effects among the constituent elements, which created more reactive sites and facilitated rapid charge transfer.

4.3.2. Hydrogen evolution reaction. In recent years, Pt and Pd-based materials have been identified as the most effective catalysts for HER,[78] displaying minimal overpotential compared to other investigated catalysts. However, these materials are expensive and, therefore, challenging to employ on a wide scale.[27] As such, non-noble transition metals and their alloys are interesting alternatives as extremely effective HER catalysts because of their partly filled *d* orbitals. Ni, Co, Fe, Cu, and Zn are non-noble metals that have weak interactions with H atoms while Mo, W, Ti, and Nb can have significant interactions with H atoms.[12,79,80] In view of these considerations, HEA-based catalysts resulting from the variable composition of these metallic elements are viable options for building affordable and effective catalysts for HER.[81] For instance, the $Ni_{20}Fe_{20}Mo_{10}Co_{35}Cr_{15}$ HEA was employed as a very stable and active electrocatalyst for HER in both acidic and basic electrolytes.[27] In contrast to Pt sheets, the HEA only required an overpotential of 107 mV in acidic solutions and 172 mV in basic solutions at a current density of 10 mA cm^{-2}. The HEA with the single phase showed much higher HER activities with exceptionally small Tafel slopes (Fig. 6a and b). Meanwhile, a quinary FeCoNiAlTi HEA has also been reported to act as a HER catalyst.[82] The prepared dendritic-like porous catalyst demonstrated excellent activity with a Tafel slope smaller than

 This journal is © The Royal Society of Chemistry 2024

Published on 20 bezna 2024. Downloaded on 01.02.2026 4:42:30.

Table 1 Performance of HEMs as electrocatalysts for the OER

HEM	Electrolyte	Overpotential	Tafel slope	Stability	Ref.
FeCoNiCrAl	1 M NaOH	317 mV@40 mA cm^{-2}	75 mV dec^{-1}	—	64
FeNiMnCrCu	1 M NaOH	342 mV@40 mA cm^{-2}	58 mV dec^{-1}	10 h@26 mA cm^{-2}	64
AlNiCoIrMo	0.5 M H_2SO_4	233 mV@10 mA cm^{-2}	55.2 mV dec^{-1}	7000 CV cycles@60 mA cm^{-2}	65
FeCoNiCuMn on carbon cloth	1.0 M KOH	263 mV@10 mA cm^{-2}	43 mV dec^{-1}	24 h@10 mA cm^{-2}	73
$FeCoNiCrNb_{0.5}$	0.1 M KOH	288 mV@10 mA cm^{-2}	27.7 mV dec^{-1}	30 h@10 mA cm^{-2}	74
FeCoNiMnCu	1.0 M KOH	280 mV@10 mA cm^{-2}	59 mV dec^{-1}	40 h@10 mA cm^{-2}	75
$(CoNiMnZnFe)_3O_{3.2}$	1.0 M KOH	336 mV@10 mA cm^{-2}	47.5 mV dec^{-1}	20 h@10 mA cm^{-2}	66
$FeNiCoCrMnS_2$	1.0 M KOH	199 mV@10 mA cm^{-2}	39.1 mV dec^{-1}	55 h@500 mA cm^{-2}	67
$(Cr_{0.2}Mn_{0.2}Fe_{0.2}Co_{0.2}Ni_{0.2})_3O_4$	1.0 M KOH	332 mV@10 mA cm^{-2}	54.5 mV dec^{-1}	20 h@10 mA cm^{-2}	76
NiFeCoMnAl oxide	1.0 M KOH	190 mV@10 mA cm^{-2}	47.6 mV dec^{-1}	50 h@10 mA cm^{-2}	77
FeCoNiIrRu@CNF	0.5 M H_2SO_4	241 mV@10 mA cm^{-2}	154 mV dec^{-1}	14 h@10 mA cm^{-2}	68
CoCrFeMnNi-P	1.0 M KOH	136 mV@10 mA cm^{-2}	85.5 mV dec^{-1}	24 h@10 mA cm^{-2}	70
$Fe_5Co_4Ni_{20}Se_{36}B_x$	1.0 M KOH	279.8 mV@10 mA cm^{-2}	59.5 mV dec^{-1}	10 h@10 mA cm^{-2}	71
$K_{0.8}Na_{0.2}(MgMnFeCoNi)F_3$	1.0 M KOH	314 mV@10 mA cm^{-2}	55 mV dec^{-1}	10 h@10 mA cm^{-2}	72

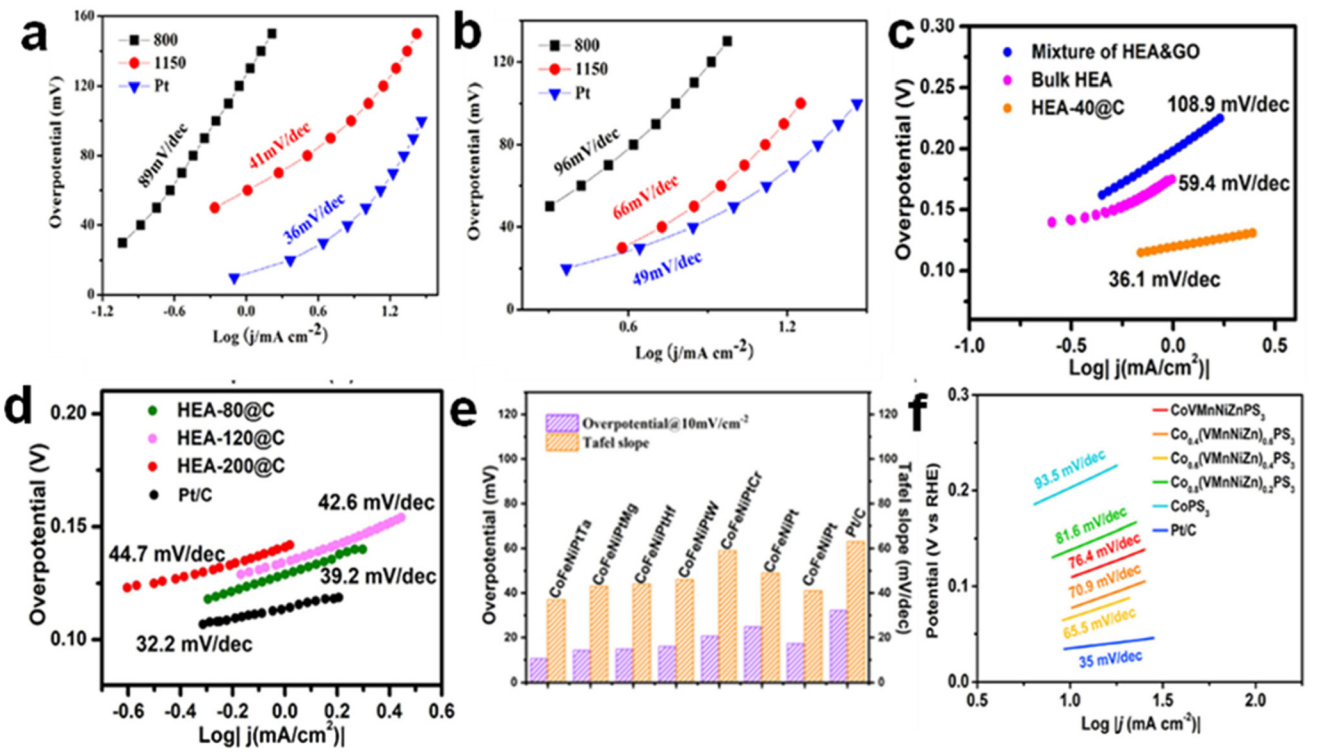

Fig. 6 Tafel plots of $Ni_{20}Fe_{20}Mo_{10}Co_{35}Cr_{15}$ in (a) 0.5 M H_2SO_4 and (b) in 1 M KOH. Reproduced from ref. 27 with permission from Elsevier, Copyright 2018. (c and d) Tafel slopes of CoNiCuMgZn-based HEAs embedded in graphene-based sheets in comparison to Pt/C catalyst. Reproduced from ref. 87 with permission from Elsevier, Copyright 2022. (e) The overpotential and Tafel slope of CoFeNiPtTa on carbon support. Reproduced from ref. 88 with permission from the American Chemical Society, Copyright 2022. (f) Tafel plots of $Co_{0.6}(VMnNiZn)_{0.4}PS_3$. Reproduced from ref. 89 with permission from the American Chemical Society, Copyright 2022.

that of the benchmark Pt sheet (79.3 mV dec^{-1}), indicating rapid kinetics of the electrocatalyst. Other HEAs like FeCoPdIrPt,[83] and $Pt_{18}Ni_{26}Fe_{15}Co_{14}Cu_{27}$ HEA[84] have also been explored for HER. Table 2 lists the HER performance of various HEMs.

Among the diverse morphological structures of HEAs, porous structures have emerged as promising electrocatalysts for water-splitting reactions. Ipadeola *et al.*[85] explored this frontier by preparing various porous HEAs with different compositions, specifically tailored for HER. Notably, their work showcased $Pt_{18}Ni_{26}Fe_{15}Co_{14}Cu_{27}/C$ as the best catalyst, boasting a low overpotential of 11 mV. Furthermore, upon extending their investigation to the OER, porous CoCrFeNiMo, adorned with phosphates, demonstrated a commendable overpotential of 220 mV. Similarly, employing ultrathin two-dimensional (2D) materials as a substrate in the development of HEAs represents a promising approach to boost HER performance.[86] For instance, CoNiCuMgZn HEA embedded in graphene

Table 2 Performance of HEMs as electrocatalysts for the HER

HEM	Electrolyte	Overpotential	Tafel slope	Stability	Ref.
$Ni_{20}Fe_{20}Mo_{10}Co_{35}Cr_{15}$	0.5 M H_2SO_4	107 mV (acidic solutions)@10 mA cm^{-2}	41 mV dec^{-1}	8 h@100 mA cm^{-2}	27
	1.0 M KOH	172 mV (basic solution)@10 mA cm^{-2}	66 mV dec^{-1}	—	
PtAuPdRhRu	0.1 M NaOH	190 mV@30 mA cm^{-2}	62 mV dec^{-1}	8 h@100 mA cm^{-2}	89
CoFeLaNiPt	0.1 M KOH	536 ± 3 mV@10 mA cm^{-2}	149 mV dec^{-1}	1 h@10 mA cm^{-2}	90
FeCoNiAlTi	1.0 M KOH	88.2 mV@10 mA cm^{-2}	40.1 mV dec^{-1}	40 h@100 mA cm^{-2}	82
NiCoFePtRh	0.5 M H_2SO_4	27 mV@10 mA cm^{-2}	30.1 mV dec^{-1}	85 h@10 mA cm^{-2}	91
FeCoNiCuPd	1.0 M KOH	29 mV@10 mA cm^{-2}	47.2 mV dec^{-1}	36 h@100 mA cm^{-2}	60
FeCoPdIrPt@GO	1.0 M KOH	42 mV@10 mA cm^{-2}	82 mV dec^{-1}	150 h@10 mA cm^{-2}	83
$Pt_{18}Ni_{26}Fe_{15}Co_{14}Cu_{27}$/C	1 M KOH + 1 M CH_3OH	11 mV@10 mA cm^{-2}	30 mV dec^{-1}	10 h@10 mA cm^{-2}	84
CoNiCuMgZn HEA embedded onto graphene sheets	1 M KOH	158 mV@10 mA cm^{-2}	36.1 mV dec^{-1}	100 h@10 mA cm^{-2}	87
CoFeNiPtTa on C	0.5 M H_2SO_4	10.6 mV@10 mA cm^{-2}	37 mV dec^{-1}	20 h@10 mA cm^{-2}	88
$Co_{0.6}(VMnNiZn)_{0.4}PS_3$	1 M KOH	65.9 mV@10 mA cm^{-2}	65.5 mV dec^{-1}	12 h@10 mA cm^{-2}	92

Published on 20 bezna 2024. Downloaded on 01.02.2026 4:42:30.

sheets exhibited an overpotential of 158 mV at a current density of 10 mA cm^{-2}.[87] Also, the Tafel slope of 36.1 mV dec^{-1} is comparable to the commercial Pt/C (32.2 mV dec^{-1}) (Fig. 6c and d). In another experimental investigation, a CoFeNiPtTa alloy on carbon support was used as a bifunctional catalyst in HER and OER tests[88] and in both instances, it demonstrated exceptional electrocatalytic prowess and stability, showcasing overpotentials of 10.6 mV and 290 mV respectively at 10 mA cm^{-2} (Fig. 6e). Furthermore, efforts have also been devoted to improve the performance of HEAs by integrating them with chalcogens. For example, 2D high-entropy metal phosphorus trichalcogenides were used as HER catalysts.[92] The synthesized $Co_{0.6}(VMnNiZn)_{0.4}PS_3$ demonstrated enhanced HER performance with an overpotential of 65.9 mV at a current density of 10 mA cm^{-2} and a Tafel slope of 65.5 mV dec^{-1} (Fig. 6f). The incorporation of chalcogen elements like S on the edge and P on the basal plane of HEAs can significantly enhance their HER performance by providing more active sites for hydrogen adsorption and promoting water dissociation during the reaction. Additionally, the vast specific surface area of 2D materials, combined with the exceptional physicochemical properties of HEAs, contribute to a larger number of catalytic active sites for HER. Overall, these distinct HEA composites offer interesting opportunities for active catalyst design and screening, as well as a platform for alternative materials research and development for water splitting reactions.

4.3.3 Oxygen reduction reaction. The oxygen reduction reaction (ORR) stands as a pivotal process in the advancement of fuel cell technology, drawing significant scientific attention worldwide. It involves the reduction of oxygen molecules to water or other species. However, its sluggish kinetics poses a formidable challenge, impeding the practical application of fuel cells and metal–O_2 batteries.[63,93] While platinum-based NPs have traditionally served as highly active ORR electrocatalysts, their prohibitive cost and limited natural resources hinder widespread implementation. In response to this challenge, researchers have turned their focus towards developing noble metal-free or low noble metal loading electrocatalysts. HEMs have emerged as promising candidates in this quest, offering a unique avenue for achieving superior catalytic performance. Several studies have showcased the potential of HEMs in catalyzing the ORR with remarkable efficiency. Löffler *et al.*[94] introduced CrMnFeCoNi NPs as non-noble metal catalysts, demonstrating comparable catalytic performance to commercial Pt/C catalysts. Additionally, Batchelor *et al.*[95] reported the exceptional catalytic activity of $Ir_{10.2}Pd_{32.0}Pt_{9.30}Rh_{19.6}Ru_{28.9}$ HEAs, which exhibit a near-continuous distribution of adsorption energies, leading to lower overpotentials compared to Pt/C catalysts. Furthermore, recent studies have highlighted the synthesis of uniform and small-sized PtFeCoNiCu HEA NPs, exhibiting superior mass activity and durability over state-of-the-art Pt/C catalysts.[96] The optimized surface electronic configuration reduces the activation barriers for breaking the O–O bond, leading to a substantial increase in the rate of the ORR process. Moreover, nanoporous AlCuNiPtMn HEAs, with low Pt loadings, has been demonstrated as effective catalysts for ORR,[97] surpassing commercial Pt/C catalysts in terms of both half-wave potential and mass activity.

More recently, the utilization of hollow high-entropy MOFs has emerged as a promising avenue. Hu *et al.*[98] have contributed to this field by developing a porous hollow high-entropy MOF-74, comprising a unique combination of Mn, Fe, Co, Ni, Cu, and Zn metal elements. The novel hollow structure of the MOF-74 framework provided multiple internal chambers and channels, facilitating efficient mass transport. Furthermore, the exploration of HEOs as catalysts for ORR has yielded promising results. In a recent investigation, researchers synthesized a series of HEO NPs consisting of ten metal elements, including Hf, Zr, La, V, Ce, Ti, Nd, Gd, Y, and Pd.[99] These NPs were uniformly deposited on commercial carbon-based powder substrates. The resulting electrocatalyst, termed 10-HEO/C, exhibited remarkable activity and, importantly, demonstrated superior stability in the ORR. After 12 and 100 h, the 10-HEO/C catalyst retained 92% and 86% of its initial activity, respectively, outperforming commercial Pd/C catalysts, which retained only 76% of their activity after 12 h. Recent efforts have also focused on the development of structurally ordered HEA NPs embedded in a nitrogen-rich mesoporous carbon

 This journal is © The Royal Society of Chemistry 2024

Published on 20 bezna 2024. Downloaded on 01.02.2026 4:42:30.

framework.[100] These catalysts demonstrate enhanced performance, featuring a substantial half-wave potential of 0.90 eV and exceptional durability, with minimal decay of 0.01 V after 10 000 cycles. This performance surpassed disordered HEA and commercial Pt/C catalysts, attributed to its improved mass transfer rates, electron conductivity, and stable chemically ordered HEA phases. Overall, the utilization of HEMs for ORR holds great promise for addressing the challenges associated with traditional catalysts, offering a pathway toward developing efficient, cost-effective, and sustainable electrocatalytic systems for various energy applications.

4.3.4 Ammonia decomposition reaction. Hydrogen offers significant promise as a clean and efficient fuel for the future but faces challenges in transportation and storage due to its extremely low density.[101] Overcoming these obstacles involves storing hydrogen in chemical compounds. To this end, NH_3 is a potential hydrogen carrier due to its high energy density, simplifying transportation and storage compared to gaseous hydrogen.[102,103] Furthermore, during the process of producing hydrogen through decomposition, gaseous NH_3 does not release any greenhouse gases into the atmosphere (Fig. 7a).[104] However, an efficient catalyst is required for the decomposition of ammonia to generate hydrogen. While Ru stands out as the most effective metal catalyst for expediting the decomposition of NH_3, its scarcity and elevated cost hinder its extensive use.[105] Recently, there has been investigation into employing HEAs for the ammonia decomposition reaction (ADR). In particular, quinary CoMoFeNiCu NPs synthesized in a single solid-solution phase were utilized as a catalyst for the ADR.[106] With an optimized Co/Mo ratio, the HEA-$Co_{25}Mo_{45}$ exhibited a mass-specific rate of 22.1 g NH_3 g metals^{-1} h^{-1} at 500 °C, with an activation energy of 64.7 kJ mol^{-1} (Fig. 7b). The rate-limiting factors in the breakdown of NH_3 were also studied. On Co-rich surfaces, the binding of N was too weak, leading to higher kinetic barriers for dehydrogenation, whereas, on Mo-rich surfaces, the binding was too strong, preventing N from recombining and desorbing from the surface. A trade-off between these two factors resulted in an ideal binding energy for the reaction. The multiple elements used in this HEA served as a promising method to overcome the stability problem. Consequently, the HEA exhibited significantly increased catalytic activity and stability compared to bimetallic Co/Mo and Ru catalysts.

In another study, the suitability of RuRhCoNiIr for NH_3 decomposition was investigated.[107] Ru and non-noble metal Ni have strong catalytic activity for NH_3 decomposition but have a significant immiscibility gap, which makes it difficult to tune binary RuNi continuously. In order to boost the entropy of the system and aid in the development of single-phase alloys, Rh, Co, and Ir were chosen. Due to their strong synergistic activity, compact size, and alloy phase, RuRhCoNiIr demonstrated good NH_3 conversion efficiency (Fig. 7c), highlighting the need for composition management and homogeneous mixing for performance optimization. Additionally, it was found that the particles were well disseminated and remained to be defined by the alloy structure after the catalytic process. Indeed, the studies showcasing the potential and successful use of HEAs for ADR are highly promising and significant for the development of clean and efficient hydrogen production processes.

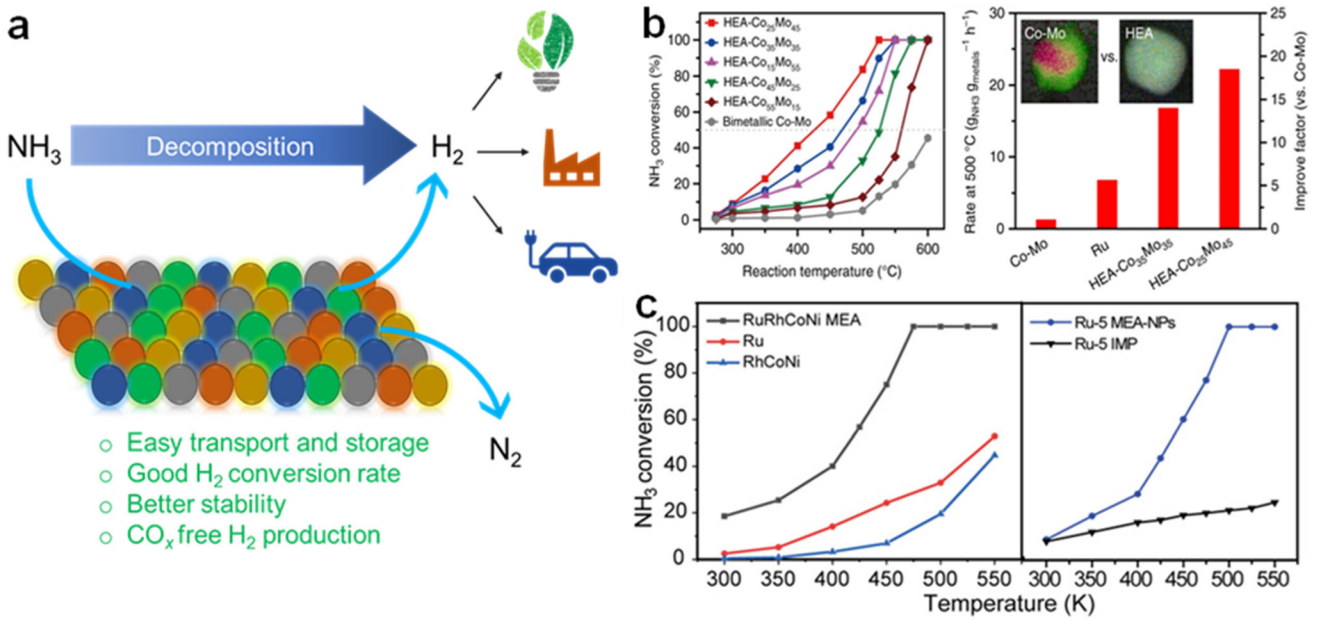

Fig. 7 (a) Illustration of the NH_3 decomposition reaction and the advantages of using HEAs as a catalyst for H_2 production. (b) NH_3 conversions over different HEA-Co_xMo_y NPs with bimetallic Co–Mo and corresponding reaction rates. Reproduced from ref. 106 with permission from Springer Nature, Copyright 2019. (c) Polarization curves of RuRhCoNiIr compared to other alloys. Reproduced from ref. 107 with permission from The American Association for the Advancement of Science, Copyright 2022.

Published on 20 bezna 2024. Downloaded on 01.02.2026 4:42:30.

4.4. Energy storage

4.4.1. Batteries. The pursuit of sustainable energy solutions has driven significant advancements in energy storage technologies. Lithium-ion batteries (LIBs) have emerged as the forefront solution due to their long cycle life, high efficiency, and lack of memory effect.[108] However, the increasing demand for energy storage surpasses the capabilities of traditional electrode materials, necessitating innovative approaches to enhance energy density. One promising strategy to overcome the limitations of traditional electrode materials involves the design of multi-cation oxides. Sarkar *et al.*[109] demonstrated the effectiveness of this approach by developing $(Co_{0.2}Cu_{0.2}Mg_{0.2}Ni_{0.2}Zn_{0.2})O$ as an anode material for LIBs. This material exhibited a remarkable capacity of 590 mA h g^{-1} and maintained a coulombic efficiency > 99% after 500 cycles. The incorporation of diverse cations enables a conversion reaction, while certain cations serve to maintain the structural integrity, ensuring long-term stability. In another study, Zheng *et al.*[110] prepared $(CrMnFeCoNi)_3O_4$, which demonstrated a reversible capacity of 596.5 mA h g^{-1} and >99% coulombic efficiency over 1200 cycles. The abundance of trivalent/quaternary ions and high oxygen vacancy concentration facilitate electron transport during charging and discharging, while the structural robustness ensures crystal integrity, even under stress conditions. In a recent investigation, researchers developed porous hollow nanofibers of $(NiCoCuFeMg)_3O_4$ for anode material of LIB.[111] It was observed that the porous structure significantly facilitated lithium ion diffusion, with each metal ion within H–F–HEO contributed uniquely to its performance: Ni^{2+}, Co^{2+}, and Cu^{2+} supported reversible capacity, Fe^{2+} influenced high-rate characteristics, and Mg^{2+} stabilized the crystal structure. Notably, the porous HEO exhibited a remarkable reversible capacity of 907 mA h g^{-1} and maintained nearly 100% of its initial capacity even under a high current density of 2 A g^{-1} for over 300 cycles. Researchers have also explored high entropy perovskite titanates for LIB anode materials. Yan *et al.*[112] synthesized the high-entropy perovskite oxide $[(Bi,Na)_{0.2}(La,Li)_{0.2}(Ce,K)_{0.2}Ca_{0.2}Sr_{0.2}]TiO_3$ with a capacity of 120.4 mA h g^{-1} after 300 cycles at 1000 mA g^{-1}.

Moreover, HEMs have been also utilized as cathode materials for LIBs. For instance, Wang *et al.*[113] reported $(Li_x(Co_{0.2}Cu_{0.2}Mg_{0.2}Ni_{0.2}Zn_{0.2})OF_x)$, a lithium-containing high-entropy fluorine oxide, exhibiting superior electrochemical properties compared to conventional metal fluorine oxides. The high configurational entropy stabilizes the structure, enhancing the specific capacity and maintaining the coulombic efficiency. Furthermore, Lun *et al.*[114] designed high-entropy LIB cathodes with a rock-salt structure, showing enhanced energy density and rate capability. By incorporating multiple transition metal species, such as $Li_{1.3}Mn^{2+}_{0.1}Co^{2+}_{0.1}Mn^{3+}_{0.1}Cr^{3+}_{0.1}Ti_{0.1}Nb_{0.2}O_{1.7}F_{0.3}$ (TM6), they achieved excellent rate capability of 307 mA h g^{-1} at a low rate of 20 mA g^{-1} and 170 mA h g^{-1} at a high rate of 2000 mA g^{-1}.

In addition to their use in LIBs, HEMs are employed as electrodes in sodium-ion batteries (NIBs). The energy storage principles of NIBs closely resemble those of LIBs, offering advantages such as ample resources, cost-effectiveness, and safety.[115] Zhao *et al.*[116] developed a layered oxide $NaNi_{0.12}Cu_{0.12}Mg_{0.12}Fe_{0.15}Co_{0.15}Mn_{0.1}Ti_{0.1}Sn_{0.1}Sb_{0.04}O_2$ that exhibited an impressive capacity retention of 83% at 3 C for 500 cycles, along with a coulombic efficiency exceeding 99%. The entropy-stabilized structure formed by multiple transition metals played a crucial role in promoting the layered structure and improving cycling stability. Furthermore, the study of multi-elemental and Na-deficient layered oxide cathodes, such as $Na_{0.83}Li_{0.1}Ni_{0.25}Co_{0.2}Mn_xTi_xSn_{0.45-2x}O_{2-\delta}$, showcased the active role of configurational entropy in comprehensively enhancing the performance of cathode materials.[117] By regulating inert cations, Mn^{4+}, Ti^{4+}, and Sn^{4+}, researchers achieved greater Na^+ transport kinetics, electrochemical reversibility, and an extended cycle life, leading to higher energy density.

Lithium–sulfur batteries (LSBs) represent another frontier in energy storage technology, offering high theoretical specific capacity, low cost, and environmental friendliness. However, practical applications of LSBs encounter issues, such as sulfur and Li_2S insulation and the notorious shuttle effect.[118] Zheng *et al.*[119] introduced the concept of high entropy to the design of cathodes for LSBs, showcasing the potential of HEOs in mitigating these challenges. The development of (NiMgCuZnCo)O as a cathode material demonstrated homogeneous dispersion of multiple metal active substances, facilitating the confinement of lithium polysulfides and promoting redox reactions in LSB cathodes. The interactions between HEO and lithium polysulfides effectively mitigated the shuttling phenomenon, enhancing the stability and performance of LSBs. Moreover, the hybridization of HEA NPs with reduced graphene oxide (rGO) is observed to improve the LSB performance.[120] FeCoNiCrMn HEA NPs exhibited synergistic interactions between multiple metal cations, leading to strong chemical confinement and fast conversion kinetics of soluble lithium polysulfides. The integration with rGO provided a conductive network to expedite Li^+ diffusion, resulting in excellent reaction kinetics and high discharge capacity even at high rates. These findings collectively highlight the potential of HEMs to revolutionize the performance of different batteries, by addressing key challenges and paving the way for their widespread adoption in future energy storage applications.

4.4.2. Supercapacitors. Electrochemical energy storage systems, such as supercapacitors, play a vital role in meeting the growing energy demand by efficiently storing and distributing energy.[121] These devices store energy by polarising the electrolyte.[122] Due to their high power density, quick charging time, and extended lifespan, they have garnered significant attention.[123] Researchers have explored diverse materials for supercapacitor electrodes, striving to boost their specific capacitance, conductivity, and specific surface area for greater energy storage capacity and quicker charge/discharge rates. Despite these efforts, optimization of the electrode materials still remains critical. Recently, HEAs have been found to be compelling candidates for supercapacitors because of their advantage of combining nanocrystalline structures with good

 This journal is © The Royal Society of Chemistry 2024

Published on 20 bezna 2024. Downloaded on 01.02.2026 4:42:30.

electrochemical performance (Fig. 8a). Notably, the electrochemical performance of the AlCoCrFeNi electrode was studied in an alkaline electrolyte.[124] The as-prepared HEA exhibited a high volumetric capacitance of ~700 F cm^{-3} (Fig. 8b) and retained 97% of its capacitance after 3000 cycles (Fig. 8c). The active oxide surface and highly conductive metal core were credited for the exceptional performance. Meanwhile, HEOs along with carbon nanotubes (CNTs) were also explored as electrochemical capacitors.[125] For instance, the AlCoCrFeNi HEO-CNT nanocomposite exhibited a high specific capacitance of 286 F g^{-1} at a scan rate of 10 mV s^{-1} (Fig. 8d). These results imply that the integration of a carbonized thin metal oxide coated HEA potentially boosts the specific capacitance and ultimately enhances the overall performance of supercapacitors.

With the idea that deposition of a HEA on aligned CNFs (ACNFs) will improve the performance of capacitors by promoting homogeneous mass and charge transport across the electrode/electrolyte interface, FeNiCoMnMg HEA NPs/ACNFs were employed as electrodes for supercapacitors.[126] It exhibited impressive capacitive performance in terms of energy density and specific capacitance as depicted in Fig. 8e. In another study, FeCoNiCuSn NPs with a thin metal oxide layer were deposited onto hyper crosslinked polymer-based carbon and

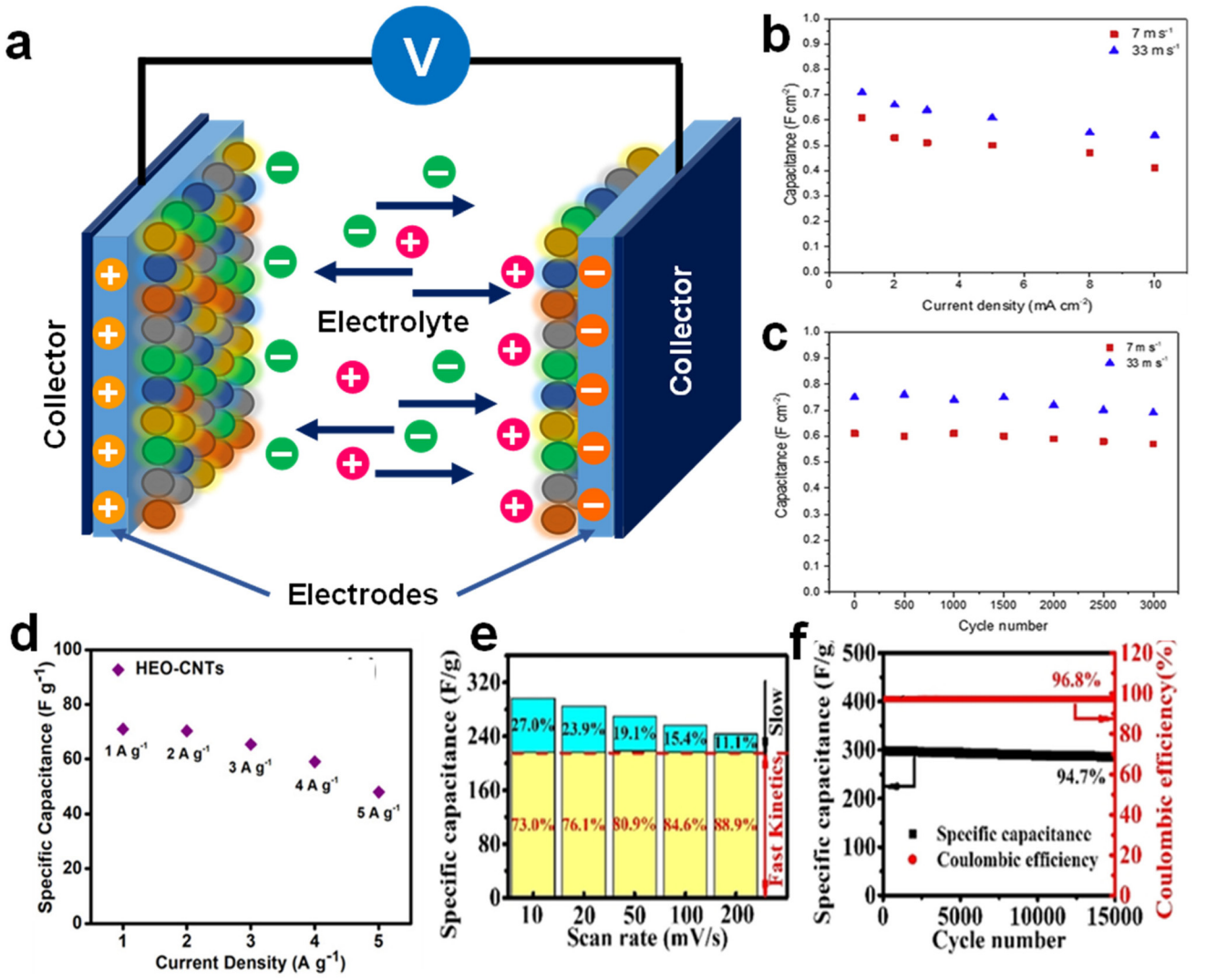

Fig. 8 (a) Structure of a supercapacitor employing HEAs as electrodes. The area-specific capacitance of AlCoCrFeNi HEA as a function of (b) current density and (c) cycle number (at a constant current density of 1 mA cm^{-2}). Reproduced from ref. 124 with permission from Elsevier, Copyright 2019. (d) Rate capability plot at different current densities for AlCoCrFeNi HEO-CNT composites. Reproduced from ref. 133 with permission from the American Chemical Society, Copyright 2019. (e) Comparison of the capacitance contributions between the fast (yellow region) and slow kinetic processes (blue region) at various scan rates and (f) the cycling performance of FeCoNiCuSn NPs with metal oxide layer deposited onto hyper crosslinked polymer-based carbon (at 10 A g^{-1}) for 15 000 cycles. Reproduced from ref. 127 with permission from John Wiley and Sons, Copyright 2021.

Table 3 Performance of HEMs as electrodes for supercapacitors

HEM	Electrolyte	Capacitance	Current/energy density	Stability	Ref.
AlCoCrFeNi	2 M KOH	700 F cm^{-3}	1 mA cm^{-2}	97% after 3000 cycles	124
FeCoNiCuZn	3 M KOH	325 F g^{-1}	1 A g^{-1}	80% after 5000 cycles	132
AlCoCrFeNi HEO-CNT	Polyvinyl alcohol/H_2SO_4 hydrogel	286 F g^{-1}	1 A g^{-1}	100% after 15 000 cycles	133
FeNiCoMnMg HEA NPs/ACNFs	6 M KOH	203 F g^{-1}	21.7 W h kg^{-1}	85% after 2000 cycles	134
FeCoNiCuSn onto hyper crosslinked polymer-based carbon	1.0 M KOH	495.4 F g^{-1}	0.5 A g^{-1}	94.7% after 15 000 cycles	127
$(FeCoCrMnZn)_3O_4$	1 M KOH	340 F g^{-1}	5 A g^{-1}	82.8% after 1000 cycles	135
$(CrMnFeCoNi)_3O_4$	2 M KOH	239 F g^{-1}	0.5 A g^{-1}	76% after 1000 cycles	128
(VCrNbMoZr)N	1 M KOH	230 F g^{-1}	—	—	129
(TiNbTaZrHf)C	$CaCl_2$	95.2 F g^{-1}	1 A g^{-1}	87% after 2000 cycles	130
MnO_2 decorated $FeCrCoMnNiAl_{0.75}$	0.5 M Na_2SO_4	961 F g^{-1}	5 A g^{-1}	81% after 6000 cycles	131

Published on 20 bezna 2024. Downloaded on 01.02.2026 4:42:30.

tested as supercapacitor electrodes.[127] The as-prepared composites exhibit ultrafast charge transport kinetics (Fig. 8f), with an excellent specific capacitance of 495.4 F g^{-1} in 1 M KOH. Furthermore, it demonstrated superior cycling stability of 94.7 % after 15 000 cycles (Fig. 8g). The pseudo capacitance of the metal oxide layer, which spontaneously developed on the outermost surface of the composite is thought to be the cause of these superior electrochemical characteristics.

Besides HEAs, their oxides have also demonstrated significant potential as electrode materials for supercapacitors. For example, spinel $(CrMnFeCoNi)_3O_4$ NPs displayed a capacitance of 239 F g^{-1} at a current density of 0.5 A g^{-1}.[128] Researchers have also explored the electrochemical behavior of various other HEA-based electrodes, including high entropy nitrides,[129] high entropy carbides,[130] and HEA metallic framework adorned with MnO_2,[131] among others as listed in Table 3. These efforts are vital for developing efficient and sustainable energy storage solutions to meet the increasing demand of high-performance supercapacitors in various applications.

5. Conclusion and outlook

In conclusion, the exploration of HEMs in catalytic applications, including the ORR, OER, HER, ADR, and organic pollutant degradation through electrocatalytic and photocatalytic processes, as well as their utilization in batteries and supercapacitors for energy storage, reflects a dynamic and promising field of current global interest. However, the operational system of HEMs is significantly more complicated as the number of components rises compared to their monometallic and bimetallic equivalents.[136,137] Therefore, as we navigate through the multifaceted landscape of HEM applications, several critical recommendations emerge for future exploration and enhancement of the functionalities of these materials.

·First, elucidating the catalytic mechanisms of HEMs and unravelling the distinctive roles of each component in catalytic processes appear pivotal. Computational approaches like high-throughput techniques, machine learning, and DFT calculations offer expedited avenues for designing and developing novel HEM-based catalysts.[138–140] Despite the complexity arising from the multicomponent composition of HEMs, further advancements in sophisticated computer-aided theoretical calculations and predictive methodologies hold promise for catalytic applications.

·Second, exploring innovative methods to discern the geometric configurations of surface atoms in HEMs is imperative. The various geometric configurations display different chemisorption behaviors toward reactants or intermediates.[141,142] It should be noted that the examination of the geometric arrangement of surface atoms in HEMs is quite difficult because of the many components and the dispersion of metal atoms. Therefore, novel research techniques, including statistical approaches, machine learning, and big data analysis, are essential for unravelling the intricate geometric layouts of active centres within the complex structures of HEMs.

·Third, understanding the influence of supporting chemicals and interfaces on catalytic performance remains crucial. Several interfaces, such as the HEM–metal, HEM–metal oxide, HEM–carbon, HEM–polymer, and so on, arise when an HEM interacts with different materials. Investigating various supporting materials for immobilizing HEMs and manipulating the atomic and electronic structure interfaces can enhance the number of active centres, improve selectivity for desired products, and manage reactant adsorption modes. Strategies such as incorporating lattice flaws as active sites and developing nano-morphologies to augment surface areas hold potential for enhancing HEA catalytic activities.

·Fourth, integrating theoretical calculations with experimental synthesis aids in predicting and optimizing the catalytic performance of HEMs. The vast compositional space of HEMs necessitates the use of theoretical simulations, especially in predicting electronic structures, d-band centres, charge transfer, and surface charge distributions.[143,144] The synergy between theory and experimentation will certainly expedite the discovery and optimization of HEMs with enhanced catalytic performance.

·Finally, simplifying the synthesis processes for HEMs is vital for practical applicability. Facile and optimized synthesis procedures are essential to streamline the sample preparation. The facile procedures should offer advantages in terms of

 This journal is © The Royal Society of Chemistry 2024

Published on 20 bezna 2024. Downloaded on 01.02.2026 4:42:30.

speed, scalability, and ease of implementation. The choice of method also depends on the specific requirements and the desired properties of the HEM. Phase engineering in HEMs allows for tailored composition and microstructures, catering to specific application requirements, further enhancing their versatility.

Needless to say, HEMs can accomplish cross-disciplinary application in numerous fields by making use of the high synergy and transformation capacity between different element combinations. As the understanding of HEMs and their behaviour advances through research and experimentation, the potential for their real-world applications will continue to grow. Interdisciplinary collaboration among materials scientists and engineers, physicists, chemists, and other experts will be essential to unlock the full potential of HEMs and bring these innovative materials into practical use. The development and successful implementation of HEMs in diverse domains have the potential to revolutionize various industries and contribute to a more sustainable and technologically advanced future.

Author contributions

Shubhasikha Das: conceptualization, methodology, formal analysis, investigation, and writing – original draft. Shamik Chowdhury: writing – review and editing and supervision. Chandra Sekhar Tiwary: writing – review and editing and supervision.

Conflicts of interest

The authors declare no competing financial interest.

Acknowledgements

C.S.T acknowledges Core research grant of SERB, India, STARS projects by MHRD-India, DAE Young Scientist Research Award (DAEYSRA), and AOARD (Asian Office of Aerospace Resarch and Development) grant no. FA2386-21-1-4014, and Naval research board for funding support.

References

1 J. W. Yeh, S. K. Chen, S. J. Lin, J. Y. Gan, T. S. Chin, T. T. Shun, C. H. Tsau and S. Y. Chang, *Adv. Eng. Mater.*, 2004, **6**, 299–303.
2 B. Cantor, I. T. H. Chang, P. Knight and A. J. B. Vincent, *Mater. Sci. Eng., A*, 2004, **375–377**, 213–218.
3 B. Wang, Y. Yao, X. Yu, C. Wang, C. Wu and Z. Zou, *J. Mater. Chem. A*, 2021, **9**, 19410–19438.
4 Z. Tang, T. Yuan, C. W. Tsai, J. W. Yeh, C. D. Lundin and P. K. Liaw, *Acta Mater.*, 2015, **99**, 247–258.
5 D. Li, C. Li, T. Feng, Y. Zhang, G. Sha, J. J. Lewandowski, P. K. Liaw and Y. Zhang, *Acta Mater.*, 2017, **123**, 285–294.
6 N. K. Katiyar, K. Biswas, J.-W. Yeh, S. Sharma and C. S. Tiwary, *Nano Energy*, 2021, **88**, 106261.
7 T. Jin, X. Sang, R. R. Unocic, R. T. Kinch, X. Liu, J. Hu, H. Liu, S. Dai, T. Jin, X. F. Liu, J. Hu, H. L. Liu, S. Dai, X. H. Sang, R. R. Unocic and R. T. Kinch, *Adv. Mater.*, 2018, **30**, 1707512.
8 P. Sarker, T. Harrington, C. Toher, C. Oses, M. Samiee, J. P. Maria, D. W. Brenner, K. S. Vecchio and S. Curtarolo, *Nat. Commun.*, 2018, **9**, 4980.
9 C. M. Rost, E. Sachet, T. Borman, A. Moballegh, E. C. Dickey, D. Hou, J. L. Jones, S. Curtarolo and J. P. Maria, *Nat. Commun.*, 2015, **6**, 8485.
10 J. Zhang, C. Cai, G. Kim, Y. Wang and W. Chen, *npj Comput. Mater.*, 2022, **8**, 89.
11 X. Wang, W. Guo and Y. Fu, *J. Mater. Chem. A*, 2021, **9**, 663–701.
12 Y. Xin, S. Li, Y. Qian, W. Zhu, H. Yuan, P. Jiang, R. Guo and L. Wang, *ACS Catal.*, 2020, **10**, 11280–11306.
13 Y. Wang and Y. Wang, *Nano Energy*, 2022, **104**, 107958.
14 Y. Wang, J. Zhang, T. Wu and G. Huang, *Ceram. Int.*, 2024, **50**, 5893–5913.
15 M. Fu, X. Ma, K. Zhao, X. Li and D. Su, *iScience*, 2021, **24**, 102177.
16 X. Wang, W. Guo and Y. Fu, *J. Mater. Chem. A*, 2021, **9**, 663–701.
17 S. Kumar and M. Kumar, *Trans. Indian Natl. Acad. Eng.*, 2024, DOI: 10.1007/s41403-023-00447-2.
18 B. Mondal, X. Zhang, S. Kumar, F. Long, N. K. Katiyar, M. Kumar, S. Goel and K. Biswas, *Nanoscale*, 2023, **15**, 17097–17104.
19 K. M. B. Urs, N. K. Katiyar, R. Kumar, K. Biswas, A. K. Singh, C. S. Tiwary and V. Kamble, *Nanoscale*, 2020, **12**, 11830–11841.
20 V. R. Naganaboina, M. Anandkumar, A. S. Deshpande and S. G. Singh, *Sens. Actuators, B*, 2022, **357**, 131426.
21 V. R. Naganaboina, M. Anandkumar, A. S. Deshpande and S. G. Singh, *ACS Appl. Nano Mater.*, 2022, **5**, 4524–4536.
22 V. Jishnu, S. S. Mishra, K. U. Mb, S. P. Thomas, C. S. Tiwary, K. Biswas and V. B. Kamble, *ACS Appl. Mater. Interfaces*, 2022, **14**, 13653–13664.
23 A. R. Ahmady, A. Ekhlasi, A. Nouri, M. H. Nazarpak, P. Gong and A. Solouk, *Smart Mater. Manuf.*, 2023, **1**, 100009.
24 D. Kumar, R. Seetharam and K. Ponappa, *J. Alloys Compd.*, 2024, **972**, 172732.
25 S. Nellaiappan, N. K. Katiyar, R. Kumar, A. Parui, K. D. Malviya, K. G. Pradeep, A. K. Singh, S. Sharma, C. S. Tiwary and K. Biswas, *ACS Catal.*, 2020, **10**, 3658–3663.
26 S. Das, M. Sanjay, A. R. Singh Gautam, R. Behera, C. S. Tiwary and S. Chowdhury, *J. Environ. Manage.*, 2023, **342**, 118081.
27 G. Zhang, K. Ming, J. Kang, Q. Huang, Z. Zhang, X. Zheng and X. Bi, *Electrochim. Acta*, 2018, **279**, 19–23.

Published on 20 bezna 2024. Downloaded on 01.02.2026 4:42:30.

28 Y. Yao, Z. Huang, P. Xie, S. D. Lacey, R. J. Jacob, H. Xie, F. Chen, A. Nie, T. Pu, M. Rehwoldt, D. Yu, M. R. Zachariah, C. Wang, R. Shahbazian-Yassar, J. Li and L. Hu, *Science*, 2018, **359**, 1489–1494.
29 N. K. Katiyar, K. Biswas, J.-W. Yeh, S. Sharma and C. S. Tiwary, *Nano Energy*, 2021, **88**, 106261.
30 Q. Guo, X. Xu, X. Pei, Z. Duan, P. K. Liaw, H. Hou and Y. Zhao, *J. Mater. Res. Technol.*, 2023, **22**, 3331–3339.
31 VOSviewer, VOSviewer - Visualizing scientific landscapes, **https://www.vosviewer.com/**.
32 N. K. Katiyar, S. Dhakar, A. Parui, P. Gakhad, A. K. Singh, K. Biswas, C. S. Tiwary and S. Sharma, *ACS Catal.*, 2021, **11**, 14000–14007.
33 S. Gao, Y. Lin, X. Jiao, Y. Sun, Q. Luo, W. Zhang, D. Li, J. Yang and Y. Xie, *Nature*, 2016, **529**, 68–71.
34 X. Zheng, P. De Luna, F. P. García de Arquer, B. Zhang, N. Becknell, M. B. Ross, Y. Li, M. N. Banis, Y. Li, M. Liu, O. Voznyy, C. T. Dinh, T. Zhuang, P. Stadler, Y. Cui, X. Du, P. Yang and E. H. Sargent, *Joule*, 2017, **1**, 794–805.
35 S. Akrami, Y. Murakami, M. Watanabe, T. Ishihara, M. Arita, M. Fuji and K. Edalati, *Appl. Catal., B*, 2022, **303**, 120896.
36 X. Wang, Y. Pan, Z. Zhu and J. Wu, *Chemosphere*, 2014, **117**, 638–643.
37 Y. Xu, T. Liu, Y. Zhang, F. Ge, R. M. Steel and L. Sun, *J. Mater. Chem. A*, 2017, **5**, 12001–12014.
38 M. Patel, R. Kumar, K. Kishor, T. Mlsna, C. U. Pittman and D. Mohan, *Chem. Rev.*, 2019, **119**, 3510–3673.
39 T. Wang, Y. Wang, N. Wang, S. Xu, Z. Han and Y. Wang, *Mater. Lett.*, 2021, **283**, 128817.
40 S. Das, M. Sanjay, S. Kumar, S. Sarkar, C. S. Tiwary and S. Chowdhury, *Chem. Eng. J.*, 2023, **476**, 146719.
41 Y. Wang, H. Zhao, M. Li, J. Fan and G. Zhao, *Appl. Catal., B*, 2014, **147**, 534–545.
42 N. Wang, *Surf. Interfaces*, 2022, **33**, 102265.
43 Y. Bai, L. Wang, Q. Tao, S. Lu, A. Zhang, K. Li and N. Hu, *J. Water Process Eng.*, 2023, **56**, 104392.
44 W. Liao, J. Wang, G. Ni, K. Liu, C. Liu, S. Chen, Q. Wang, Y. Chen, T. Luo, X. Wang, Y. Wang, W. Li, T. S. Chan, C. Ma, H. Li, Y. Liang, W. Liu, J. Fu, B. Xi and M. Liu, *Nat. Commun.*, 2024, **15**, 1264.
45 I. Katsounaros, M. Dortsiou and G. Kyriacou, *J. Hazard. Mater.*, 2009, **171**, 323–327.
46 P. H. van Langevelde, I. Katsounaros and M. T. M. Koper, *Joule*, 2021, **5**, 290–294.
47 M. Yang, T. Wei, J. He, Q. Liu, L. Feng, H. Li, J. Luo and X. Liu, *Nano Res.*, 2024, **17**, 1209–1216.
48 C. J. M. Van Der Ham, M. T. M. Koper and D. G. H. Hetterscheid, *Chem. Soc. Rev.*, 2014, **43**, 5183–5191.
49 B. H. R. Suryanto, H. L. Du, D. Wang, J. Chen, A. N. Simonov and D. R. MacFarlane, *Nat. Catal.*, 2019, **2**, 290–296.
50 Z. Song, Y. Liu, Y. Zhong, Q. Guo, J. Zeng, Z. Geng, Z. Song, Y. Liu, Y. Zhong, J. Zeng, Z. Geng and Q. Guo, *Adv. Mater.*, 2022, **34**, 2204306.
51 P. Li, Z. Jin, Z. Fang and G. Yu, *Energy Environ. Sci.*, 2021, **14**, 3522–3531.
52 L. X. Li, W. J. Sun, H. Y. Zhang, J. L. Wei, S. X. Wang, J. H. He, N. J. Li, Q. F. Xu, D. Y. Chen, H. Li and J. M. Lu, *J. Mater. Chem. A*, 2021, **9**, 21771–21778.
53 Q. Gao, H. S. Pillai, Y. Huang, S. Liu, Q. Mu, X. Han, Z. Yan, H. Zhou, Q. He, H. Xin and H. Zhu, *Nat. Commun.*, 2022, **13**, 2338.
54 J. M. Walls, J. S. Sagu and K. G. Upul Wijayantha, *RSC Adv.*, 2019, **9**, 6387–6394.
55 Y. F. Yu, W. Zhang, Q. J. Fang, X. L. Zhang, S. T. Zhao, W. X. Chen and G. L. Zhuang, *Appl. Surf. Sci.*, 2023, **626**, 157246.
56 S. Sun, C. Dai, P. Zhao, S. Xi, Y. Ren, H. R. Tan, P. C. Lim, M. Lin, C. Diao, D. Zhang, C. Wu, A. Yu, J. C. J. Koh, W. Y. Lieu, D. H. L. Seng, L. Sun, Y. Li, T. L. Tan, J. Zhang, Z. J. Xu and Z. W. Seh, *Nat. Commun.*, 2024, **15**, 260.
57 C. Dues, W. G. Schmidt and S. Sanna, *ACS Omega*, 2019, **4**, 3850–3859.
58 Z. Abbas, N. Hussain, I. Ahmed and S. M. Mobin, *Inorg. Chem.*, 2023, **62**, 8835–8845.
59 D. Zhou, P. Li, X. Lin, A. McKinley, Y. Kuang, W. Liu, W. F. Lin, X. Sun and X. Duan, *Chem. Soc. Rev.*, 2021, **50**, 8790–8817.
60 S. Wang, B. Xu, W. Huo, H. Feng, X. Zhou, F. Fang, Z. Xie, J. K. Shang and J. Jiang, *Appl. Catal., B*, 2022, **313**, 121472.
61 Y. Lee, J. Suntivich, K. J. May, E. E. Perry and Y. Shao-Horn, *J. Phys. Chem. Lett.*, 2012, **3**, 399–404.
62 F. Meng, H. Zhong, J. Yan and X. Zhang, *Nano Res.*, 2017, **10**, 4436–4447.
63 J. T. L. Gamler, K. Shin, H. M. Ashberry, Y. Chen, S. L. A. Bueno, Y. Tang, G. Henkelman and S. E. Skrabalak, *Nanoscale*, 2020, **12**, 2532–2541.
64 X. Cui, B. Zhang, C. Zeng and S. Guo, *MRS Commun.*, 2018, **8**, 1230–1235.
65 Z. Jin, J. Lv, H. Jia, W. Liu, H. Li, Z. Chen, X. Lin, G. Xie, X. Liu, S. Sun and H. J. Qiu, *Small*, 2019, **15**, 1904180.
66 Y. Zhang, W. Dai, P. Zhang, T. Lu and Y. Pan, *J. Alloys Compd.*, 2021, **868**, 159064.
67 T. X. Nguyen, Y.-H. Su, C.-C. Lin, J.-M. Ting, T. X. Nguyen, Y.-H. Su, C.-C. Lin and J.-M. Ting, *Adv. Funct. Mater.*, 2021, **31**, 2106229.
68 H. Zhu, Z. Zhu, J. Hao, S. Sun, S. Lu, C. Wang, P. Ma, W. Dong and M. Du, *Chem. Eng. J.*, 2022, **431**, 133251.
69 Y. Yao, Z. Ma, Y. Dou, S. Y. Lim, J. Zou, E. Stamate, J. O. Jensen and W. Zhang, *Chem. – Eur. J.*, 2022, **28**, e202104288.
70 X. Zhao, Z. Xue, W. Chen, Y. Wang and T. Mu, *ChemSusChem*, 2020, **13**, 2038–2042.
71 Y. Zuo, D. Rao, S. Ma, T. Li, Y. H. Tsang, S. Kment and Y. Chai, *ACS Nano*, 2019, **13**, 11469–11476.
72 T. Wang, H. Chen, Z. Yang, J. Liang and S. Dai, *J. Am. Chem. Soc.*, 2020, **142**, 4550–4554.
73 K. Huang, B. Zhang, J. Wu, T. Zhang, D. Peng, X. Cao, Z. Zhang, Z. Li and Y. Huang, *J. Mater. Chem. A*, 2020, **8**, 11938–11947.

 This journal is © The Royal Society of Chemistry 2024

Published on 20 bezna 2024. Downloaded on 01.02.2026 4:42:30.

74 Z. Ding, J. Bian, S. Shuang, X. Liu, Y. Hu and C. Sun, *Adv. Sustainable Syst.*, 2020, **4**, 1900105.
75 K. Huang, D. Peng, Z. Yao, J. Xia, B. Zhang, H. Liu, Z. Chen, F. Wu, J. Wu and Y. Huang, *Chem. Eng. J.*, 2021, **425**, 131533.
76 Z. Sun, Y. Zhao, C. Sun, Q. Ni, C. Wang and H. Jin, *Chem. Eng. J.*, 2022, **431**, 133448.
77 M. Han, C. Wang, J. Zhong, J. Han, N. Wang, A. Seifitokaldani, Y. Yu, Y. Liu, X. Sun, A. Vomiero and H. Liang, *Appl. Catal., B*, 2022, **301**, 120764.
78 W. Li, K. Liu, S. Feng, Y. Xiao, L. Zhang, J. Mao, Q. Liu, X. Liu, J. Luo and L. Han, *J. Colloid Interface Sci.*, 2024, **655**, 726–735.
79 P. Ma, M. Zhao, L. Zhang, H. Wang, J. Gu, Y. Sun, W. Ji and Z. Fu, *J. Mater.*, 2020, **6**, 736–742.
80 H. Shen, T. Wei, Q. Liu, S. Zhang, J. Luo and X. Liu, *J. Colloid Interface Sci.*, 2023, **634**, 730–736.
81 Q. Zhang, K. Lian, G. Qi, S. Zhang, Q. Liu, Y. Luo, J. Luo and X. Liu, *Sci. China Mater.*, 2023, **66**, 1681–1701.
82 Z. Jia, T. Yang, L. Sun, Y. Zhao, W. Li, J. Luan, F. Lyu, L.-C. Zhang, J. J. Kruzic, J.-J. Kai, J. C. Huang, J. Lu and C. T. Liu, *Adv. Mater.*, 2020, **32**, 2000385.
83 S. Gao, S. Hao, Z. Huang, Y. Yuan, S. Han, L. Lei, X. Zhang, R. Shahbazian-Yassar and J. Lu, *Nat. Commun.*, 2020, **11**, 2016.
84 H. Li, Y. Han, H. Zhao, W. Qi, D. Zhang, Y. Yu, W. Cai, S. Li, J. Lai, B. Huang and L. Wang, *Nat. Commun.*, 2020, **11**, 5437.
85 A. K. Ipadeola, A. K. Lebechi, L. Gaolatlhe, A. B. Haruna, M. Chitt, K. Eid, A. M. Abdullah and K. I. Ozoemena, *Electrochem. Commun.*, 2022, **136**, 107207.
86 C. Qin, S. Chen, H. Gomaa, M. A. Shenashen, S. A. El-Safty, Q. Liu, C. An, X. Liu, Q. Deng and N. Hu, *Acta Phys. – Chim. Sin.*, 2024, **40**, 2307059.
87 D. Feng, Y. Dong, P. Nie, L. Zhang and Z. A. Qiao, *Chem. Eng. J.*, 2022, **430**, 132883.
88 H. Chen, C. Guan and H. Feng, *ACS Appl. Nano Mater.*, 2022, **5**, 9810–9817.
89 M. Liu, Z. Zhang, F. Okejiri, S. Yang, S. Zhou and S. Dai, *Adv. Mater. Interfaces*, 2019, **6**, 1900015.
90 M. W. Glasscott, A. D. Pendergast, S. Goines, A. R. Bishop, A. T. Hoang, C. Renault and J. E. Dick, *Nat. Commun.*, 2019, **10**, 2650.
91 G. Feng, F. Ning, J. Song, H. Shang, K. Zhang, Z. Ding, P. Gao, W. Chu and D. Xia, *J. Am. Chem. Soc.*, 2021, **143**, 17117–17127.
92 R. Wang, J. Huang, X. Zhang, J. Han, Z. Zhang, T. Gao, L. Xu, S. Liu, P. Xu and B. Song, *ACS Nano*, 2022, **16**, 3593–3603.
93 Q. Zhang, K. Lian, Q. Liu, G. Qi, S. Zhang, J. Luo and X. Liu, *J. Colloid Interface Sci.*, 2023, **646**, 844–854.
94 T. Löffler, H. Meyer, A. Savan, P. Wilde, A. Garzón Manjón, Y. T. Chen, E. Ventosa, C. Scheu, A. Ludwig and W. Schuhmann, *Adv. Energy Mater.*, 2018, **8**, 1802269.
95 T. A. A. Batchelor, J. K. Pedersen, S. H. Winther, I. E. Castelli, K. W. Jacobsen and J. Rossmeisl, *Joule*, 2019, **3**, 834–845.
96 T. Chen, F. Ning, J. Qi, G. Feng, Y. Wang, J. Song, T. Yang, X. Liu, L. Chen and D. Xia, *iScience*, 2023, **26**, 105890.
97 S. Li, X. Tang, H. Jia, H. Li, G. Xie, X. Liu, X. Lin and H. J. Qiu, *J. Catal.*, 2020, **383**, 164–171.
98 J. Hu, L. Cao, Z. Wang, J. Liu, J. Zhang, Y. Cao, Z. Lu and H. Cheng, *Compos. Commun.*, 2021, **27**, 100866.
99 T. Li, Y. Yao, B. H. Ko, Z. Huang, Q. Dong, J. Gao, W. Chen, J. Li, S. Li, X. Wang, R. Shahbazian-Yassar, F. Jiao and L. Hu, *Adv. Funct. Mater.*, 2021, **31**, 2010561.
100 G. Zhu, Y. Jiang, H. Yang, H. Wang, Y. Fang, L. Wang, M. Xie, P. Qiu and W. Luo, *Adv. Mater.*, 2022, **34**, 2110128.
101 N. K. Katiyar, S. Nellaiappan, R. Kumar, K. D. Malviya, K. G. Pradeep, A. K. Singh, S. Sharma, C. S. Tiwary and K. Biswas, *Mater. Today Energy*, 2020, **16**, 100393.
102 F. Schüth, R. Palkovits, R. Schlögl and D. S. Su, *Energy Environ. Sci.*, 2012, **5**, 6278–6289.
103 S. Wang, F. Ichihara, H. Pang, H. Chen, J. Ye, S. Wang, F. Ichihara, H. Pang, J. Ye and H. Chen, *Adv. Funct. Mater.*, 2018, **28**, 1803309.
104 T. V. Choudhary, C. Sivadinarayana and D. W. Goodman, *Catal. Lett.*, 2001, **72**, 197–201.
105 S. F. Yin, Q. H. Zhang, B. Q. Xu, W. X. Zhu, C. F. Ng and C. T. Au, *J. Catal.*, 2004, **224**, 384–396.
106 P. Xie, Y. Yao, Z. Huang, Z. Liu, J. Zhang, T. Li, G. Wang, R. Shahbazian-Yassar, L. Hu and C. Wang, *Nat. Commun.*, 2019, **10**, 4011.
107 Y. Yao, Z. Liu, P. Xie, Z. Huang, T. Li, D. Morris, Z. Finfrock, J. Zhou, M. Jiao, J. Gao, Y. Mao, J. Miao, P. Zhang, R. Shahbazian-Yassar, C. Wang, G. Wang and L. Hu, *Sci. Adv.*, 2020, **6**, 510–523.
108 B. Scrosati and J. Garche, *J. Power Sources*, 2010, **195**, 2419–2430.
109 A. Sarkar, L. Velasco, D. Wang, Q. Wang, G. Talasila, L. de Biasi, C. Kübel, T. Brezesinski, S. S. Bhattacharya, H. Hahn and B. Breitung, *Nat. Commun.*, 2018, **9**, 3400.
110 B. Xiao, G. Wu, T. Wang, Z. Wei, Y. Sui, B. Shen, J. Qi, F. Wei and J. Zheng, *Nano Energy*, 2022, **95**, 106962.
111 X. L. Wang, E. M. Kim, T. G. Senthamaraikannan, D.-H. Lim and S. M. Jeong, *Chem. Eng. J.*, 2024, **484**, 149509.
112 J. Yan, D. Wang, X. Zhang, J. Li, Q. Du, X. Liu, J. Zhang and X. Qi, *J. Mater. Sci.*, 2020, **55**, 6942–6951.
113 Q. Wang, A. Sarkar, D. Wang, L. Velasco, R. Azmi, S. S. Bhattacharya, T. Bergfeldt, A. Düvel, P. Heitjans, T. Brezesinski, H. Hahn and B. Breitung, *Energy Environ. Sci.*, 2019, **12**, 2433–2442.
114 Z. Lun, B. Ouyang, D. H. Kwon, Y. Ha, E. E. Foley, T. Y. Huang, Z. Cai, H. Kim, M. Balasubramanian, Y. Sun, J. Huang, Y. Tian, H. Kim, B. D. McCloskey, W. Yang, R. J. Clément, H. Ji and G. Ceder, *Nat. Mater.*, 2020, **20**, 214–221.
115 P. Wang, B. Xi, Z. Zhang, M. Huang, J. Feng and S. Xiong, *Angew. Chem., Int. Ed.*, 2021, **60**, 15563–15571.

Published on 20 bezna 2024. Downloaded on 01.02.2026 4:42:30.

116 C. Zhao, F. Ding, Y. Lu, L. Chen and Y. S. Hu, *Angew. Chem., Int. Ed.*, 2020, **59**, 264–269.
117 H. Wang, X. Gao, S. Zhang, Y. Mei, L. Ni, J. Gao, H. Liu, N. Hong, B. Zhang, F. Zhu, W. Deng, G. Zou, H. Hou, X. Y. Cao, H. Chen and X. Ji, *ACS Nano*, 2023, **17**, 12530–12543.
118 S. Di, S. Chen, C. Chang, S. Wang, J. Choi and L. Li, *Scr. Mater.*, 2023, **226**, 115218.
119 Y. Zheng, Y. Yi, M. Fan, H. Liu, X. Li, R. Zhang, M. Li and Z. A. Qiao, *Energy Storage Mater.*, 2019, **23**, 678–683.
120 Y. Yao, Z. Zhao, R. Niu, J. Chen and X. Wang, *Chem. Phys. Lett.*, 2024, **839**, 141124.
121 K. Nabeela, R. Deka, Z. Abbas, P. Kumar, M. Saraf and S. M. Mobin, *Cryst. Growth Des.*, 2023, **23**, 3057–3078.
122 S. Huang, X. Zhu, S. Sarkar and Y. Zhao, *APL Mater.*, 2019, **7**, 100901.
123 S. N. Ansari, M. Saraf, Z. Abbas and S. M. Mobin, *Nanoscale*, 2023, **15**, 13546–13560.
124 K. Kong, J. Hyun, Y. Kim, W. Kim and D. Kim, *J. Power Sources*, 2019, **437**, 226927.
125 M. S. Lal and R. Sundara, *ACS Appl. Mater. Interfaces*, 2019, **11**, 30846–30857.
126 X. Xu, Y. Du, C. Wang, Y. Guo, J. Zou, K. Zhou, Z. Zeng, Y. Liu and L. Li, *J. Alloys Compd.*, 2020, **822**, 153642.
127 E. Shen, X. Song, Q. Chen, M. Zheng, J. Bian and H. Liu, *ChemElectroChem*, 2021, **8**, 260–269.
128 B. Talluri, M. L. Aparna, N. Sreenivasulu, S. S. Bhattacharya and T. Thomas, *J. Energy Storage*, 2021, **42**, 103004.
129 T. Jin, X. Sang, R. R. Unocic, R. T. Kinch, X. Liu, J. Hu, H. Liu and S. Dai, *Adv. Mater.*, 2018, **30**, 1707512.
130 J. Sure, D. Sri Maha Vishnu, H.-K. Kim and C. Schwandt, *Angew. Chem., Int. Ed.*, 2020, **59**, 11830–11835.
131 Y. Yuan, Z. Xu, P. Han, Z. Dan, F. Qin and H. Chang, *J. Alloys Compd.*, 2021, **870**, 159523.
132 G. C. Mohanty, C. Chowde Gowda, P. Gakhad, S. Das, M. Sanjay, S. Chowdhury, K. Biswas, A. Singh and C. S. Tiwary, *Electrochim. Acta*, 2023, **470**, 143272.
133 M. S. Lal and R. Sundara, *ACS Appl. Mater. Interfaces*, 2019, **11**, 30846–30857.
134 X. Xu, Y. Du, C. Wang, Y. Guo, J. Zou, K. Zhou, Z. Zeng, Y. Liu and L. Li, *J. Alloys Compd.*, 2020, **822**, 153642.
135 B. Liang, Y. Ai, Y. Wang, C. Liu, S. Ouyang and M. Liu, *Mater*, 2020, **13**, 5798.
136 Z. W. She, J. Kibsgaard, C. F. Dickens, I. Chorkendorff, J. K. Nørskov and T. F. Jaramillo, *Science*, 2017, **355**, eaad4998.
137 L. Zhou, D. F. Swearer, C. Zhang, H. Robatjazi, H. Zhao, L. Henderson, L. Dong, P. Christopher, E. A. Carter, P. Nordlander and N. J. Halas, *Science*, 2018, **362**, 69–72.
138 Y. J. Hsu, W. C. Chiang and J. K. Wu, *Mater. Chem. Phys.*, 2005, **92**, 112–117.
139 N. Kumar, Q. Ying, X. Nie, R. S. Mishra, Z. Tang, P. K. Liaw, R. E. Brennan, K. J. Doherty and K. C. Cho, *Mater. Des.*, 2015, **86**, 598–602.
140 D. Roy, S. C. Mandal and B. Pathak, *ACS Appl. Mater. Interfaces*, 2021, **13**, 56151–56163.
141 Y. Wang, L. Cao, N. J. Libretto, X. Li, C. Li, Y. Wan, C. He, J. Lee, J. Gregg, H. Zong, D. Su, J. T. Miller, T. Mueller and C. Wang, *J. Am. Chem. Soc.*, 2019, **141**, 16635–16642.
142 H. Li, K. Shin and G. Henkelman, *J. Chem. Phys.*, 2018, **149**, 174705.
143 B. Hammer and J. K. Nørskov, *Surf. Sci.*, 1995, **343**, 211–220.
144 X. Du, J. Huang, J. Zhang, Y. Yan, C. Wu, Y. Hu, C. Yan, T. Lei, W. Chen, C. Fan and J. Xiong, *Angew. Chem., Int. Ed.*, 2019, **58**, 4484–4502.

 This journal is © The Royal Society of Chemistry 2024